12-2003

Modeling of Circulation Zone and Shear Layers in Coaxial Injectors

Clayton Andrew White
University of Tennessee - Knoxville

To the Graduate Council:

I am submitting herewith a thesis written by Clayton Andrew White entitled "Modeling of Circulation Zone and Shear Layers in Coaxial Injectors." I have examined the final electronic copy of this thesis for form and content and recommend that it be accepted in partial fulfillment of the requirements for the degree of Master of Science, with a major in Engineering Science.

Charles Merkle, Major Professor

We have read this thesis and recommend its acceptance:

Basil Antar, Gary Flandro

Accepted for the Council:
Carolyn R. Hodges

Vice Provost and Dean of the Graduate School

(Original signatures are on file with official student records.)

To the Graduate Council:

I am submitting herewith a thesis written by Clayton Andrew White entitled "Modeling of Circulation Zone and Shear Layers in Coaxial Injectors." I have examined the final electronic copy of this thesis for form and content and recommend that it be accepted in partial fulfillment of the requirements for the degree of Master of Science, with a major in Engineering Science.

Charles Merkle

Charles Merkle, Major Professor

We have read this thesis and
recommend its acceptance:

Basil Antar

Gary Flandro

Acceptance for the Council:

Anne Mayhew

Vice Provost and Dean of
Graduate Studies

(Original signatures are on file with official student records.)

MODELING OF CIRCULATION ZONE AND SHEAR LAYERS IN COAXIAL INJECTORS

A Thesis

Presented for the

Master of Science

Degree

The University of Tennessee, Knoxville

Clayton A. White

December 2003

DEDICATION

This thesis is dedicated to my wife, Shelia, and my two daughters, Hannah and Emily, whose pride in my work inspires me to continue the struggle to learn and understand.

ACKNOWLEDGMENTS

I would like to thank the people that were instrumental in helping me complete my Master of Science degree in Engineering Science. I thank Dr. Charles Merkle for his expertise in CFD and his patience as I strive to learn the concepts. Thanks to Dr. Basil Antar for systematically laying the basis of my fluid mechanics training and to Dr. Gary Flandro for his methodical instruction in compressible flows. I would also like to thank Dr. Ding Li for his training in running parallel computations and his generous supply of GEMS code and support utilities.

ABSTRACT

Gaseous/gaseous hydrogen oxygen shear coaxial injectors were modeled to investigate grid parameters affecting solution and to determine if a steady state solution might exist if only one circulation zone was present. The General Equation Mesh Solver (GEMS), which implements the Reynolds Averaged Navier-Stokes equations with the k-ω turbulence model, was used to conduct the study. The Gambit grid generator was used to construct computational grids. Different grids were compared in a search for the optimum configuration while residual levels were monitored in search of a steady state solution.

TABLE OF CONTENTS

LIST OF TABLES

LIST OF FIGURES

Chapter 1. Introduction

1.1 Background

There has been considerable interest in shear coaxial injectors in recent years for applications in rocket engines. One focus has been to create computational models that accurately predict the experimental results thus far obtained. While making many advances in computational fluid dynamics, the engineering/scientific community still does not accurately predict all aspects of these injectors. This thesis is one step of many toward a better prediction of this turbulent reacting flow. Previous research as well as this work are based on gas/gas hydrogen oxygen injectors. A description of this geometry is in order.

A cross-section of a multi-element injection system is shown in Figure 1. This figure and all other figures are provided in the Appendix. Although only three injectors are pictured in this figure, there may be several hundred in a typical assembly. Naturally, this would require a staggering amount of computational power to accurately model such geometry. Only one element, therefore, is considered here. This single element is represented by the dotted rectangle shown around one of the injectors. Figure 2 shows a blowup of this uni-element injector with the dotted line representing the axis of symmetry for an axisymmetric calculation. A throat has been added to achieve choking. Figure 3 shows another view looking down the tubes so that coaxial nature of the injector is illustrated.

Note that Figures 1-3 are not to scale. Table 1 has a complete list of the exact dimensions used for the geometry.

A cursory examination of recent work by others is in order. The Propulsion Center at Penn State carried out a joint experimental/analytical study [1, 2, 3] in which the experiment was compared to computational solutions. Deshpande and Merkle [1] stated that computations on refined grids of chemically reacting flow fields were too computationally intensive to be of practical use at the time and focused their efforts on the impact that the unsteady nature of the flow has on global characteristics. One of their conclusions was that the unsteady nature of the flow increased with momentum ratio of the hydrogen flow to the oxygen flow but not in a monotonic manner. They also stated that the unsteadiness is local to the near field of the splitter post and becomes damped out downstream. One suggestion they give is that some artificial damping might be employed to model this flow field.

Deshpande et. al. [2] also carried out a computational study of the effects of splitter plate thickness on the flame holding characteristics of the flow. One conclusion was that the splitter plate had to be a finite thickness in order to anchor the flame without having to preheat the reactants. Studies were conducted to investigate the location of the flame in relationship to the momentum ratios of each inlet species as well as the plate thickness. In order to facilitate this study, a larger splitter plate was modeled than some of the other studies mentioned.

Table 1: Geometry Specification

Parameter	Value
Length of Oxygen Tube	0.1778m
Length of Hydrogen Annulus	0.127m
Inner Radius of Oxygen Tube	3.8735×10^{-3}m
Outer Radius of Hydrogen Annulus	6.35×10^{-3} m
Outer Radius of Oxygen Tube/Inner Radius of Hydrogen Annulus	4.7625×10^{-3}m
Hydrogen Annulus Height (Channel Height)	1.5874×10^{-3}m
Length from Injector Face to Throat	4.9275×10^{-2}m
Throat Radius	6×10^{-3}m

Three different computational groups [3] compared their solutions and found that the solutions were all similar and provided a reasonable prediction of the flow field. This conclusion was based on comparison to experimental measurements. All groups assume axisymmetry and claim that three-dimensional calculations will be feasible in the near future.

Recent advances in processor power have allowed Archambault and Peroomian [4] to carry out three-dimensional calculations and compare the fidelity of two dimensional and three-dimensional calculations. One of their conclusions was that the axisymmetric calculation captures most of the essence of the flow field reasonably well. Based on this conclusion and on site computing power, all computations for this thesis are on two dimensional axisymmetric grids.

1.2 Proposed Research Topic

The current computational power at the UT Space Institute allows parallel processing of a significant number of grid points. This capability can be employed to run a refined shear layer grid against a coarse shear layer grid to determine if the amount of error in the outer portion of the shear layer may be reduced through grid refinement as suggested by Archambault and Peroomian [4]. In order to give proper refinement in the shear layers and boundary layers, gridding schemes must be investigated in order to keep the number of grid points from going too high and overburdening the current computer configuration while

still giving proper refinement in the needed regions. Also, to keep the numerical simulation feasible, direct numerical simulation will be avoided by employing Reynolds Average Navier-Stokes equations (RANS) with the two-equation k-ω turbulence model to close the system, as described by Wilcox [6]. This is implemented in the General Equation Mesh Solver (GEMS) written by Li and Merkle [7].

Finally, the outer circulation region shown in Figure 4 by the large counterclockwise arrows is much larger than the inner circulation region depicted in the same figure by the clockwise small arrows. Note that the direction of the small arrows may not always be clockwise but yet is dependent upon the ratio of the momentum to that of the hydrogen flow to the oxygen flow. By cutting the combustion chamber off at the same radius as the hydrogen flow as seen in Figure 5, the outer circulation region can be eliminated while at the same time reducing the total number of grid points. This will allow examination of the inner circulation region without the interference of the outer circulation zone. The isolation of the inner circulation zone will allow for a search of a steady state solution to determine if the unsteady effects are due solely to the outer recirculation zone or if some of the unsteadiness is inherent to the inner circulation zone.

Chapter 2. Basic Solution Tools

2.1 General Equation Mesh Solver

The General Equation Mesh Solver (GEMS) written by Li and Merkle [7] was the software employed to obtain the flow field solutions. This solver is an implicit unstructured solver allowing for two or three-dimensional calculations. Two-dimensional calculations can be carried out either in axisymmetric or planar form. All calculations in this thesis were done using two-dimensional axisymmetric calculations.

The basic general equation form solved by the software is as follows.

$$\frac{\partial Q}{\partial \tau} + \frac{\partial F_i}{\partial x_i} = 0 \qquad (2.1)$$

Where $Q = (\rho, \rho u, \rho v, \rho w, \rho h^0 - p)^T$ and the flux vectors F_i are the conservative flux vectors and τ is a pseudo-time variable for marching.

2.2 Chemistry

The solver allows for multiple species in chemically reacting flow. Finite rate reactions using the Arrhenius Law were used in this study [13]. Thermodynamic data, transport data, and binary diffusivity data were taken from industry compiled files [7-12]. The particular model used was an 18 equation, 9 species model listed below. The species used are H_2, O_2, OH, H_2O, H, O, HO_2, H_2O_2, and N_2 and the reversible reactions are

$H_2 + OH \Leftrightarrow H_2O + H$

$O_2 + H \Leftrightarrow OH + O$

$H_2 + O \Leftrightarrow OH + H$

$O_2 + H + N2 \Leftrightarrow HO_2 + N_2$

$H_2 + N_2 \Leftrightarrow H + H + N_2$

$O_2 + N_2 \Leftrightarrow O + O + N_2$

$H + HO_2 \Leftrightarrow H_2 + O_2$

$H_2O + N_2 \Leftrightarrow OH + H + N_2$

$H_2O + O \Leftrightarrow 2OH$

$O + HO_2 \Leftrightarrow O_2 + OH$

$H + HO_2 \Leftrightarrow 2OH$

$OH + HO_2 \Leftrightarrow O_2 + H_2O$

$H_2 + HO_2 \Leftrightarrow H + H_2O_2$

$OH + H_2O_2 \Leftrightarrow H_2O + HO_2$

$2HO_2 \Leftrightarrow O_2 + H_2O_2$

$H + H_2O_2 \Leftrightarrow OH + H_2O$

$H_2O_2 + N_2 \Leftrightarrow 2OH + N_2$

$H + O + N_2 \Leftrightarrow OH + N_2$

2.3 Two-equation k-ω Turbulence Model

The shear coaxial fuel injector scenario is a turbulent problem. Direct numerical simulation of this problem is beyond the scope of the current computers. Fortunately, GEMS allows for the calculation of either laminar flows or turbulent flows. The latter option avoids the computational intensity of direct numerical simulation by using the k-ω turbulence model where k is the kinetic energy and ω is the turbulence frequency as described by Wilcox [6]. This is a two-equation model that brings closure to the Reynolds Average Navier-Stokes equations (RANS).

2.4 Hardware

The hardware used to run the current software configuration consists of a Beowulf cluster of 50, 2 GHz Pentium IV processors each with a gigabyte of RAM. A fiber-optic fast switching network provides the communications backbone. To use this set up, the mesh is first partitioned with METIS from the University of Minnesota [15]. Then MPICH from Argonne National Laboratory [16] handles communication between the processors. Library calls are made to both of these packages directly from the FORTRAN 90 code in the GEMS package and associated utilities.

2.5 Gambit Grid Generator

The Gambit Grid generator from Fluent Technologies [17] was used to generate the grids for this project. A cursory comparison was conducted between XCFD-GEOM [18] and between the Gambit Grid generator [17]. The latter was selected because of greater flexibility in unstructured gridding techniques. More about this flexibility is discussed in the next two sections.

Chapter 3. Grid Generation

3.1 Parametric Study Setup

One of the main goals of this study was to achieve a grid independent solution. One way to ensure this accuracy is through proper grid refinement. Grid refinement could not be carried too far to the extreme because the solutions had to be obtained within a reasonable amount of time. The way to achieve both of these objectives was by refining the grid in areas where previous research, knowledge, and intuition had shown the most need for refinement. These areas are where high property gradients exist and grid refinement is in the direction or directions of the property gradients. Unfortunately, these regions are not always known beforehand. In other areas the grid can be coarse in order to minimize CPU time. Unstructured grids allow for that kind of flexibility and hence were useful in this case.

Parametric studies were first carried out on the oxygen tube by itself and the hydrogen annulus by itself. The purpose of these studies was to determine exactly how much grid resolution was needed in the injector section to obtain a grid independent solution. The criteria for judging the profiles was based on common configurations in every day fluid mechanics texts, specifically turbulent pipe flow for the oxygen tube and turbulent channel flow for the hydrogen annulus. Keep in mind, however, that the hydrogen annulus is not exactly a channel flow due to the axisymmetric nature of the geometry.

For the initial parametric study of the oxygen tube and the hydrogen annulus, the grids for both the oxygen tube in the hydrogen annulus were chosen to be rectangular meshes to match the straightforward rectangular geometry of the cross sections. Later, when the combustion chamber nozzle is attached to the tube and annulus, the mesh in the immediate region of exit section of the injector is no longer made a rectangular mesh. This will be explained more in detail in Chapter 4.

A short introductory grid was attached to each inlet with boundary conditions set to inviscid walls to ensure a uniform flow coming into the inlets. The remaining boundary conditions for the inlets and exits are summarized in a Table 2.

3.2 Stretching in x Direction for Oxygen Tube

As an initial step, the oxygen tube was meshed with a 146x13 grid and the flow field solved. This grid was stretched in both the x and y directions. Then the grid was doubled in refinement in both dimensions and solved to also yield solutions on 292x26, 584x52, and 1168x104 grids. Figure 6 shows the initial x stretching scheme used in contrast to a fixed Δx. In addition to the grids representing a doubling of the original 146x13 grid, a grid with stretching in both directions was also solved with dimensions of 584x104. This grid has the same y lines as the 1168x104 but only half of the x lines of that finest grid.

Table 2: Inlet and Outlet Boundary Conditions

Boundary Location	Boundary Values
Oxygen Tube Inlet	Pressure = 1.29 MPa Temperature = 297 K Mass Flow = 4.2×10^{-2} kg/s
Oxygen Tube Outlet	Back Pressure=1.29 MPa
Oxygen Tube Reynolds Number based on Diameter	3.11×10^{6}
Hydrogen Inlet	Pressure = 1.29 MPa Temperature = 297 K Mass Flow = 1.03×10^{-2} kg/s
Hydrogen Outlet	Back Pressure = 1.29 MPa
Hydrogen Annulus Reynolds Number based on Channel Height	6.24×10^{5}

A comparison of the velocity exit profile on the various grids used in the oxygen tube is shown in Figure 7. In order to avoid any interference given by the exit boundary conditions, the exit profile was actually measured at 3% of the tube length from the outlet. An important note is that the 584x104 grid exit velocity profile lies directly on top of the 1168 by 104 grid. The conclusion is that 584 is enough x points in the oxygen tube. Here it can be clearly seen that cutting the number of x grid points by 50% in this case yields the same exit velocity profile as long as the y resolution is the same.

It is also important to note at this time that the solution at the left end of the tube is of little importance. The only part that is of any interest in this case is the exit profile. A look at the friction velocity u_τ in Figure 8 shows that grids with enough Δx refinement at the inlet will resolve the transition to turbulence. The friction velocity u_τ is defined as

$$u_\tau = \sqrt{\frac{\tau_{wall}}{\rho}} \tag{3.1}$$

With τ_{wall} being the wall stress defined as

$$\tau_{wall} = \mu \frac{\partial u}{\partial y} \tag{3.2}$$

Since the wall stress is less for laminar flow, the friction velocity is also less. This gives the short dip in the friction velocity while the flow is still laminar at the inlet. Notice that grids 1168x104, 584x52, and 584x104 all show a sharp dip in

friction velocity at the inlet of the tube. Here the refinement in the x direction at the entrance has high enough resolution to model the transition to turbulence. The coarse grids do not capture this transition. The important point to note is that the resolution of this transition makes very little difference in exit velocity profile as seen from the precision of the profiles in Figure 7. Also note that in the transition region there is a slight difference in the friction velocity between the 584x104 and the 1168x104 grids. The important point to note here is that even though there is a slight difference in the transition region, the curves become identical a short distance from the transition region further supporting the idea that modeling of the transition region has very little effect on exit velocity profile.

3.3 Stretching in x Direction for Hydrogen Annulus

Computations in the hydrogen annulus give rise to similar conclusions. As an initial step in modeling the hydrogen annulus, grid stretching in the x direction was compared with uniform grid spacing. A 430x30 grid stretched in x and y and an 860x60 grid representing doubling in refinement in each dimension of the 430x30 grid was compared with an 860x60 fixed Δx grid and an 250x60 fixed Δx grid. Figure 9 shows the difference in exit velocity profiles for these grids. All three curves representing the grids that have 60 y grid points lie virtually on top of each other. This shows that the stretched 860x60 grid profile solution is no different than the 860x60 fixed Δx grid. More importantly it shows that the 250x60 fixed Δx grid gives the same exit profile as 860x60 grid. This is important in that the number of x grid points can be cut by a major amount

without affecting the exit profile. In this case a cut of 71% did not alter the exit velocity profile. This is a significant savings in grid points.

The main difference in the curve that stands by itself is that it has a different number of y grid points, 30 instead of 60 like the other grids. The conclusion, therefore, is that there is a stronger dependence of the velocity exit profile on the number y grid points than the number of x grid points in support of the idea that the grid refinement is needed only in the directions of the largest property gradients, which is in this case $\partial u/\partial y$ mostly in the boundary layer.

Figure 10 shows a friction velocity comparison of the hydrogen tube grids. The finest three grids show a pronounced dip in the friction velocity at the inlet due to the level of refinement at the inlet. The modeling of the transition to turbulence has no effect on the exit profile as can be readily seen in Figure 9 by the fact that the two grids that did not model the turbulence transition give an indistinguishable profile from the 860x60 grid that models the transition. This further solidifies the conclusion made from the oxygen tube friction velocity that the number x grid points can be cut significantly and still maintain the same exit velocity profile. Furthermore, fixed Δx grids give an identical exit velocity profile as the profiles obtained from stretched Δx grids.

3.4 Comparisons to Other Models

In order to inspect the accuracy of the oxygen tube computations, a comparison was made with several turbulence models. Figure 11 shows three popular turbulence models taken from Wilcox' enclosed disk [9] as well as a log wall approximation and the viscous sub layer approximation. All were compared with the finest 1168x104 grid on a semi log plot. The viscous sub layer region is evident in the region that deviates from the log wall approximation between 10^{-6} and 10^{-5}. The parabolic curve is the viscous sub layer approximation. This is the region where the velocity scale u^+ is approximately equal to the non-dimensional length scale y^+. The region from 10^{-5} out to the region of the velocity defect law follows closely to the log wall approximation except for the Cebeci-Smith model, which seems to overestimate the velocity. The comparison to these various models shows that the GEMS computation is in an appropriate accuracy range.

Figure 12 shows a similar comparison of the hydrogen annulus exit velocity profile to the same models. Here again the parabolic curve represents the viscous sub layer approximation. The straight line represents the log wall approximation. Although there is slight difference between all the models, the GEMS code falls fairly close to the other models.

The issue of how well developed the flow is should be raised. The oxygen tube is some 23 diameters long. Figure 13 shows a development of the velocity profile at the corresponding locations of 75% on down through 3%. The origin is placed at

the tube exit so that x = -100% would be at the inlet of the tube and x = 0 % would be at the exit of the tube. In this coordinate system the fluid flows first passed the x = -75% location and on out to the x = - 3% location to exit the tube. There is still significant development between the x = -25% location and x = - 3% location. The confidence in the amount of development of the oxygen profile can be fortified by the results in Figure 12 again showing that the GEMS computation is reasonably close to two of the other models being Baldwin-Lomax and Spallart-Allmaras which are both models of fully developed profiles. Wilcox code [6] is also for incompressible flows. At this stage of comparison, the solutions are at low enough Mach number that the incompressible approximation is valid.

The hydrogen annulus on the other hand is much more developed than the oxygen tube. The hydrogen annulus is 80 channel heights long. Figure 14 shows how well developed the flow is. Notice that on the graph the flow is developed well enough that only the x = -75% velocity profile is distinguishable from the other three and hence not fully developed yet. Once the hydrogen flow has reached the x = -50% location it is significantly developed as can be seen by the overlap of the two curves.

3.5 Stretching in the y Direction

Stretching in the y direction was utilized on all grids. The final goal was to set the first grid point off the wall to a distance corresponding to the non-dimensional length scale, $y^+=1$, in order to obtain a high degree of accuracy in the boundary

layer. Note, however, that some of the coarser grids in the initial parametric studies in sections 3.2-3.4 had first y grid point values corresponding to y^+=8 or less. The finest and final grid choices all had y^+=1. The first grid point off the wall was calculated using the following formula.

$$\frac{y}{y^+} = \frac{\mu}{\sqrt{\tau_{wall}\rho}} \tag{3.1}$$

where

$$\tau_{wall} = \frac{C_f \rho u^2}{2} \tag{3.2}$$

The variable y in 3.1 is the spacing from the wall to the first grid point that is desired. The friction coefficient C_f in 3.2 was taken from an empirical formula from White [14] as follows.

$$C_f = \frac{0.455}{\ln^2(0.06\,\mathrm{Re}_x)} \tag{3.3}$$

White gives this formula +/- 2% accuracy over the entire turbulent range. Re_x is the Reynolds number based on the length of the tube or channel. Table 3 gives the pertinent data used to compute the distance of the first grid point.

The result for oxygen was 6.356×10^{-7}m. The result for hydrogen was 1.4×10^{-6}m. This distance was so small that a fixed Δy for grid points was not at all feasible. For the oxygen tube there would be more than 6000 y grid points alone and that is only for half the tube considering the symmetry used in implementing the grid. Stretching in the y direction, therefore, was imperative if the boundary layer was

Table 3: First Δy Calculation

Variable	Description	Value
y^+	Non-dimensional length scale	1
μ (O_2)	Viscosity for Oxygen	207×10^{-7} Pa.S
μ (H_2)	Viscosity for Hydrogen	9.0×10^{-6} Pa.S
T	Temperature for both gases	298 K
C_f (O_2)	Friction Coefficient for Oxygen	2.667×10^{-3}
C_f (H_2)	Friction Coefficient for Hydrogen	2.351×10^{-3}
ρ (O_2)	Density for Oxygen	16.72 kg/m^3
ρ (H_2)	Density for Hydrogen	1.053 kg/m^3
u (O_2)	Inlet velocity for Oxygen	54 m/s
u (H_2)	Inlet velocity for Hydrogen	177 m/s

to be accurately modeled.

3.6 Final Inlet Grid Configuration

Based on the conclusions above, the final grid configuration arrived at for the oxygen tube was 350x104 fixed Δx. The number of x grid points was chosen by reducing the finest grid x resolution by 71% as was done with the hydrogen annulus. The hydrogen grid was chosen to be 250x60 with fixed Δx. The slight modifications to these parameters are discussed next.

3.7 Boundary Layer Refinement

Careful grid refinement considerations for the oxygen and hydrogen exits have been studied and now attachment of a combustion chamber grid can be implemented using the conclusions from previous sections. All boundary layers on the computational grid need refinement due to the strong velocity gradients within the layer. Figure 15 is a blowup of the computational grid geometry with labels indicating those boundary layer sections on the walls. First of all notice that the actual computational grid is only half of the geometry shown in Figure 5 due to the symmetry axis. The axis of symmetry does not need strong grid refinement in that area because the gradients are very small in the center of the tube. The other walls, however, are viscous and will have a corresponding boundary layer and must have refinement in the y direction due to the boundary layer gradients.

In previous sections the hydrogen annulus and oxygen tube boundary layers were already studied and the proper determination of the smallest Δy made on those viscous walls. The only two additional walls in the complete grid are the wall at the end of the splitter plate and the outer wall along the combustion chamber going down to the throat and out the nozzle. The velocities and other information in these regions were not known beforehand. Here intuition was used to determine the proper grid resolution in these areas. The outer wall continuing from the hydrogen annulus out to the throat and on out the nozzle was simply taken to be the same grid refinement as the boundary layer in the hydrogen annulus on its outer wall. The end of the splitter plate is a different situation altogether. The velocities close to the wall at this splitter plate may vary greatly depending upon the momentum ratio of the hydrogen flow to the oxygen flow. Since such a range of velocities might exist here depending upon the properties of the recirculation region, this particular wall was simply set at a first grid point distance value averaged between the Δy values for the hydrogen annulus and oxygen tube on their viscous wall boundary layers. This allowed for some sort of uniform transition between each of the two injector exits.

3.8 Shear Layer Refinement

Viscous walls are not the only place where there are strong velocity gradients. In this geometry strong velocity gradients will also be encountered in the shear layers whose the expanding regions enclosed by dotted lines in Figure 15 show approximate position. While these dotted lines represent the traditional view of

the shear layer, the fact that there is a finite thickness splitter plate here that allows for the inner circulation zone makes the shear layers a little less defined than an infinitesimal thickness splitter plate shear layer. The entire region of the inner circulation zone as shown in Figure 4 by the small arrows may contain strong velocity gradients at any point within that region depending on the eddy sizes. Grid refinement must be applied to that entire region also in both directions.

The need for a non-rectangular grid becomes apparent when trying to grid the shear layer sections. Figure 16 shows the result of continuing a boundary layer grid into the shear layer zone. While this technique is obviously an easy way to generate a grid rapidly, it leaves much to be desired. As the flow moves farther and farther from the splitter plate, the shear layer expands and the velocity gradients eventually began to decrease and damp out. In Figure 16, however, the grid resolution in the y direction directly off of the splitter plate boundary layer continues all the way down the chamber. The result, therefore, is too much grid resolution in too small a space at a far distance down the chamber. The grid must have the most resolution in places that need it but lesser amount of resolution in places that do not need it in order to conserve grid points.

3.9 Transitioning From Refined Areas To Coarser Areas

Unstructured grids give the flexibility to make transitions from these areas that are extremely refined into areas that are much coarser. An unstructured grid is a grid

in which the degree of each node may be different. The degree of a node is defined as the number of connecting nodes to that node. While the complete grids for this thesis are unstructured, most of the grid is actually structured. The unstructured sections are only needed to transition from refined areas to coarser areas and thereby save grid points.

Gambit [17] offers quadrilaterals and triangles as the primary cell shapes. It pieces these together in a number mapping schemes, some that include only triangles and some that include only quadrilaterals and some that are hybrid. The general procedure is to place nodes upon an edge of the geometry. There are several spacing schemes provided to the user for the edge nodes. Once the edges of the geometry are meshed, the user can employ one of the automatic mapping schemes to mesh the inside of the entire geometry at once. Unfortunately, the mapping schemes are not very robust and have a tendency to fail if the edges are meshed in such a way that will produce high aspect ratio grids. That is precisely the crux of the problem in the boundary layer; high aspect ratio cells abound.

The end of the oxygen or hydrogen tube gives a good example of the difficulty encountered in one of these transition regions. In section 3.2 it was determined that a constant Δx in the injector tube was sufficient to model a proper exit profile for either the oxygen tube or the hydrogen annulus. In those studies, however, the fluid in the tube exited into free space. When the combustion chamber is attached, there should be some interaction between the chamber pressure, shear

layer, and some of the boundary layer sections along the splitter plate close to the end of the tube. In anticipation of this interaction, the Δx should be refined along the splitter plate towards the end of the tube or the annulus. On the outer radius of the hydrogen annulus or upon the axis of symmetry of the oxygen tube the effects of the boundary layer near the exit of the tube on the splitter plate and its interaction with the inner circulation zone and shear layers should not be felt. The Δx in these regions along the axis of symmetry and the outer radius of the hydrogen annulus can and should remain constant.

Figure 17 shows a solution that Gambit offers to this region. Shown is the region at the top of the splitter plate where there is a small Δx in the hydrogen boundary layer and transitioning up through the hydrogen annulus into larger Δx on the outer radius. Δx was taken to be a constant value down both the hydrogen annulus and the oxygen tube up to 1/8 length of the tube from the combustion chamber/inlet interface. At this location Δx is gradually refined until maximum refinement is reached at the end of the hydrogen annulus or oxygen tube. Since such a small Δx was not needed on the outer radius of the hydrogen annulus, transitioning was used in order to save grid points.

In Figure 17 rectangular blocks are left visible to illustrate the methodology used in generating the grids. Each rectangle was drawn and nodes placed upon each edge. On the bottom edge there would be more nodes than there were on the top edge. Gambit used what is referred to as a 'quad pave' to make the transition. The

reason individual rectangles had to be drawn was because gambit's lack of robustness in generating the quad pave. Through trial and error the following restrictions were found to be true when using a quad pave meshing scheme. If the edge nodes were spaced so as to create high aspect ratio cells, the quad pave was very likely to fail or produce undesirable results. Also, the more cells an individual rectangle had in it, the more likely it was to produce undesirable results. As a result of these restrictions, small rectangles making small transitions had to be constructed. Obviously this procedure is not a highly automated technique at this time. The automatic quad pave procedure often failed in high aspect ratio regions where it was needed most.

Figure 18 shows a larger portion of the oxygen tube grid without the individual blocks being visible. The section shown is a portion of the coarse grid used in the computations. Figure 19 shows the similar situation in the oxygen tube transitioning at the inlet/chamber interface.

3.10 The Coarse Grid And Refined Grid

Now that a workable transitioning scheme has been employed, the shear layers can be transitioned into less refined areas to get away from the inefficiencies that were illustrated in Figure 16. Figure 20 shows the results of transitioning the shear layers into coarser areas. The remainder of this study focuses on two grids, one referred to as the coarse grid in Figure 20 and the other referred to as the refined grid in Figure 21. For both of these grids the oxygen tube and hydrogen

annulus grids were identical. The transition from refined shear layer areas into coarser areas was performed much more slowly on the refined grid in Figure 21 than the coarse grid in Figure 20 as can be seen from visual inspection. This should allow for testing to see whether shear layer refinement plays a significant role in this case.

Chapter 4. Initial and Boundary Conditions

4.1 Initial Conditions And Ignition

With the grids complete computational runs could then proceed. One of the issues is how to ignite the mixture without causing an explosion and hence causing the code to crash. A workable solution was found by setting the initial conditions in such a way as to minimize the reaction area until the run could progress far enough to reach some kind of stable flame regime. Specifically, this was accomplished by filling the oxygen tube and hydrogen annulus both at a temperature of 297 K. The oxygen tube was set with a mass fraction of 100% oxygen and the hydrogen annulus with a mass fraction of 100% hydrogen. The combustion chamber, throat, and nozzle, in contrast, were set to 1200 K with 100% mass fraction of oxygen. This gave an interface of hydrogen at 297 K at the end of the hydrogen annulus to oxygen at 1200 K at the annulus entrance into the chamber. Figure 22 shows the temperature contour at the time of ignition where that interface initiates combustion. Figure 22 also shows as time progresses the flame front beginning to wash down the chamber. Figure 23 shows the progression even further to the point of washing out the throat and eventually achieving a stable flame down the length of the combustion chamber and out the nozzle.

In order to reach a stable flame scenario, care had to be exercised to keep the code from crashing just at the point of ignition. The initial condition for oxygen at 1200 K was sufficient for igniting the reactants. The temperature at the interface

between hydrogen and oxygen quickly jumped to the temperature regime of adiabatic combustion of hydrogen and oxygen. In order to keep the code from blowing up during this time, a small CFL was chosen and linearly increased to reach the maximum CFL used during the runs. The maximum CFL for all runs was 0.1. Taking 1/100 of the maximum CFL and performing a linear increase of the CFL during each real time step so that at the 100th iteration the maximum CFL was reached accomplished the linear increase for the CFL.

4.2 Boundary Conditions

The only other conditions to be specified were the boundary conditions. The inlet conditions for the oxygen and hydrogen entrances were specified by setting a pressure, temperature, and mass flow rate. These inlet conditions were chosen based on configurations from previous experimental work [5] so that the results might fall into the same regime. The nozzle exit boundary condition was also chosen based on the previous experimental work. Table 4 shows the complete listing of the boundary conditions used on the full grid runs.

Table 4: Boundary Conditions

Boundary	Values
Oxygen Inlet	Pressure = 1.29 MPa Temperature = 297 K Mass Flow Rate = 4.2 kg/s
Hydrogen Inlet	Pressure = 1.29 MPa Temperature = 297 K Mass Flow Rate = 1.02 kg/s
Nozzle Exit	Back Pressure = 0.101 MPa

Chapter 5. Shear Layer Analysis

5.1 Profile Comparisons

Once runs had been achieved with stable flames on both the coarse and refined grids, a shear layer analysis was conducted. A location was chosen at x = 9 mm to extract a cross section profile. Remembering that the origin of x starts at the end of the splitter plate, the location of 9 mm was chosen by intuition to be far enough away from the splitter plate so as not to cross the inner circulation zone but at the same time to not be into the converging section of the nozzle. Once that location was chosen profiles were constructed by averaging the extracted profile over the last 10 frames of the run. A frame was generated by saving the results of the flow field calculation every 20 real time steps in hopes of avoiding any drastic fluctuations in the profile that could be caused from vortex shedding or flame flapping.

Figure 24 shows the velocity profile comparison at the x = 9 mm location. Notice that most of the difference in the profiles is in the shear layer region and splitter plate wake region. The Mach profile comparison in Figure 25 shows a good correlation on the boundary layer at the outer radius, but shows no particular correlation in any other region. The species profiles in Figures 26, 27, and 28, however, all show some difference within the shear layer and wake region while having very little difference in results outside of that region. This is to be expected since there is very little flow in the y direction outside the circulation zone.

The temperature profile comparison in Figure 30 shows a marked difference in the width of the high temperature region as well as the intensity. The peak intensity of the temperature on this profile has a 17% difference from one grid to the other. This should be enough to produce significantly different characteristics downstream in a larger model. Also, in Figure 31, a marked difference can be seen in the pressure profile mostly in the shear layer and wake region. There is a difference all the way across the profile in the pressure comparison, but the highest percentage of difference is found in the shear layer wake region. In Figure 32 the density profile shows the most difference in the shear layer wake region like most of the other properties do.

5.2 Grid Dependency Conclusions

In the profiles previously reviewed most of the differences in the results were located in the shear layer wake region. This is in light of the fact that grid independent solutions were obtained for the oxygen tube and hydrogen annulus independently. This is clear evidence that grid resolution in the shear layer plays a major role in the quality of the results. Furthermore, the difference in solutions at the short distance from the splitter plate could cause a major change in the solution in much longer geometries.

Chapter 6. Convergence and Unsteadiness

6.1 Convergence of Oxygen Tube and Hydrogen Annulus

One of the objectives of this study was to see if there is a steady state solution to the flow field if the outer circulation zone was eliminated. In the parametric studies conducted on oxygen tube and hydrogen annulus independently, steady state solutions were found for both of those flow fields. Figure 33 illustrates the convergence of the oxygen tube computation. Four of the runs on the oxygen tube were from grids that were doubled in each dimension. Is interesting to note that a doubling of two dimensions make some four times as many points in the grid. The number of iterations required for convergence, however, did not increase by a factor of 4. Another point to make is that the 584x52 grid and the 584x104 grid had almost identical convergence rates. This suggests that in this geometry the convergence rate was based on the x grid resolution. The aspect ratio for these two runs differ by factor of two because of decreasing the y resolution by a factor of 2, which increases the value of y + corresponding to the first grid point by a factor of two. The dominant CFL in this geometry, which affected convergence, was based on x.

The convergence rates were compared for the hydrogen annulus grids in Figure 34. Like the oxygen tube all the hydrogen grids yielded a steady state solution and were driven to machine accuracy. A similar conclusion about the convergence rate depending on the number of x grid points can be drawn from the hydrogen grids. The 860x60 stretched grid in the 860x60 fixed Δx grid had

nearly identical convergence rates. The nonlinear effects at the beginning of the run shifted the fixed Δx grid so that it achieved machine accuracy in fewer iterations than the stretched grid, but the general slopes are the same.

6.2 Convergence of Full Grids

Even though the oxygen tube and hydrogen annulus produced steady state solutions, neither of the full grids converged to a steady state solution. Figure 35 shows a comparison of the convergence between the coarse grid and refined grid. The banded appearance is produced from a dual time step solution procedure. In each real time step there would be a certain number of inner time steps. This dual time stepping produces an oscillation in the residual giving the banded look appearing in the figure. The important point to note in this figure is that the general trend of the residual between the coarse grid in the refined grid is similar. Visual inspection of the figure shows that the residual stops decreasing at around –3 and a steady state solution is not realized.

In looking for the source of the unsteadiness that causes the steady state solution to be elusive, examination of the flow field was in order. Figure 36 shows he Mach contour on the refined grid. The downwash from the wake region of the splitter plate is still apparent at the throat. As a result the sonic line is extremely curvy there. Figure 37 gives a clearer picture of this choking by showing the sonic line in the throat. This sonic condition in the wake of the splitter plate appears to tend towards going subsonic out the nozzle. Upon examination of this

sonic line the size of the throat was called in to question. The throat radius was originally chosen from the experimental geometry conducted at Penn State [5]. The difference in that geometry, however, was that the chamber was many times longer than this one which allowed time for the shear layer to expand and for the flame and temperature profile also to expand. This expansion produced a much different profile at the throat thereby insuring adequate choking in the longer chamber of the physical experiments.

A quasi 1-D analysis of this geometry requires many estimations because it is not true quasi 1-D due to property variations with respect to y. Even with estimations and averaging across the grid, it is questionable as to whether the flow field is choked. Without the combustion a quasi 1-D approximation would be more appropriate. The approximation for cold flow shows that it is not choked and can be seen in Figure 38 by examining the results of a non-reacting cold flow case. The sonic line travels into the inlets in that case.

In search of a steady state solution the throat radius from the experiments was abandoned and a quasi 1-D analysis on cold flow was computed and the throat radius set to 92% of the choking radius. The area was computed by solving the following equation [19] for the choking area, A^*

$$massflow = p_0 A^* \sqrt{\frac{\gamma}{RT_0}} \left(\frac{2}{\gamma + 1} \right)^{\frac{\gamma+1}{2(\gamma-)}} \qquad \textbf{(6.1)}$$

where the zero subscript denotes stagnation properties, γ is the ratio of specific heats, and R is the specific gas constant for the mixture. Table 5 shows the values used for the calculation.

The choking radius computed from the area was 3.23×10^{-3} m from which the throat radius was set to 92% of that value. This new geometry is shown in Figure 39 and shows that even with cold flow the flow field is now choked at the throat. Runs were then conducted on the new geometry with reacting flow to see if a steady state solution could be found for the flow field. Figure 40 shows the reacting flow field Mach contour with the smaller throat. Figure 41 shows the sonic line on the same run exhibiting much more uniformity and much less of the effects from the wake of the splitter plate. Unfortunately, this configuration still did not yield a steady state solution. Figure 42 shows the results of the residual from the new configuration compared with the previous residuals from the coarse grid and refined grids. Notice that general trends of the residual are similar to the previous geometry. Visual inspection indicates the limit of the residual has been realized.

Table 5: Parameters For Choking Radius Computation

Parameter	Value
Mass flow	0.0523 kg/s
Stagnation Pressure	1.29 MPa
Stagnation Temperature	300K
Specific Gas Constant	1020.9 J/kg.K
Ratio of Specific Heats	1.4

Chapter 7. Conclusions and Recommendations

7.1 Conclusion

Comparisons between the property profiles across the shear layers in the combustion chamber show that grid refinement changes the profile a significant amount. The differences in the profiles due to the refinement of the grid in the shear layer may alter the flow field characteristics far downstream in larger combustion chambers. In order to accurately model the shear layer sections, a high level of grid refinement is needed in the shear layer due to strong property gradients in the combustion region.

No steady state solution was found on the full computational grid flow field. Elimination of the outer circulation zone did not eliminate the unsteadiness of the flow field and indicates there is an inherent unsteadiness associated with the inner circulation zone, shear layer, and splitter plate wake.

7.2 Recommendations

Further refinement is needed in the shear layer section to compare with the refined shear layer grid used in this study in order to ascertain how close the solution on the refined grid is to being grid independent. In order to efficiently generate such grid refinements, more robust grid generation techniques or software are needed. Some other methods of analyzing unsteadiness could be employed. GEMS code could be made to make 2-D contours of the residual so that regions of unsteadiness could be readily identified. Furthermore, a longer

chamber could eliminate some of the choking problems encountered on the first two full grids.

Additional factors could also be modeled like the heat flux up the splitter plate. Eventually, 2 phase flows will need to be accurately modeled to bring the problem to a maximum level of realism.

LIST OF REFERENCES

LIST OF REFERENCES

[1] Deshpande, M., & Merkle, C., L., "Characterization of Unsteady Effects in GH2/GO2 Combustor Modeling," AIAA 96-3128, 32nd AIAA/ASME/SAE/ASEE Joint Propulsion Conference, Lake Buena Vista, FL July 1996.

[2] Deshpande, M., Venkateswaran, S., Foust, M., & Merkle, C.L., "Finite Splitter Effects on Flame Holding in a Confined Hydrogen-Oxygen Shear Layer," AIAA 97-0258, 35th Aerospace Sciences Meeting & Exhibit, Reno, NV, January 1997.

[3] Schley, C. -A., Gagemann, G., Tucker, P.K., Venkateswaran, S., & Merkle, C.L., "Comparison of Computational Codes for Modeling Hydrogen-Oxygen Injectors," AIAA 97-3302, 33rd AIAA/ASME/SAE/ASEE Joint Propulsion Conference & Exhibit, Seattle, WA, July 1997.

[4] Archambault, M. R., & Peroomian, O., "Three-Dimensional Simulations of a Gas/Gas, Hydrogen/Oxygen Engine," AIAA 2003-0314, 41st Aerospace Sciences Meeting & Exhibit, Reno, NV, January 2003.

[5] Foust, M.J., Deshpande, M., Pal, S., Ni, T., Merkle, C. L., & Santoro, R. J., "Experimental and Analytical Characterization of a Shear Coaxial Combusting GO_2/GH_2 Flowfield," AIAA 96-0646, 34th Aerospace Sciences Meeting & Exhibit, Reno, NV January 1996

[6] Wilcox, D. C., Turbulence Modeling for CFD, 2nd ed., DCW Industries, ISBN 0-9636051-5-1, 1998.

[7] Li, D. and Merkle, C. L., "Convergence Assessment of General Fluid Equations on Unstructured Hybrid Grids," AIAA 2001-2557.

[8] Li, D. and Merkle, C. L., "CFD Analysis of Leakage Characteristics of Labyrinth Seals in a Steam Turbine," FEDSM2001-18060.

[9] Li, D. and Merkle, C. L., "Application of a General Structured-Unstructured Solver to Flows of Arbitrary Fluids," ICCFD 2000.

[10] Li, D. and Merkle, C. L., "Unstructured Methods in CFD," Final report to AEDC, 2001.

[11] Gordon, S., and McBride, B.J. "Computer Program for Calculation of Complex Chemical Equilibrium Compositions, and Applications." NASA RP-1311, Part I and II, 1994.

[12] Kee, R. J., Dixon-Lewis, G., Warnatz, J., Coltrin, M.E., and Miller, J.A., "A FORTRAN Computer Code Package for the Evaluation of Gas-Phase, Multicomponent Transport Properties," SAND86-8246, Dec. 1986.

[13] Turns, S.R., An Introduction to Combustion: Concepts and Applications, 2nd ed., St. Louis: McGraw-Hill, 2000.

[14] White, F. M., Viscous Fluid Flow, NY: McGraw-Hill, 1974.

[15] Karypis, G, "METIS: Family of Multilevel Partitioning Algorithms," [Online Downloadable Software Library], Mar. 2002, Available HTTP: http://www-users.cs.umn.edu/~karypis/metis/

[16] "MPICH – A Portable Implementation of MPI," [Online Downloadable Software Library], Jan. 2003, Available HTTP: http://www-unix.mcs.anl.gov/mpi/mpich/

[17] "Gambit 2.0.4," [Grid Generation Software], 2003, Fluent Inc., HTTP: http://www.fluent.com/

[18] "CFD-GEOM 6.6.0.18," [Grid Generation Software], 2000, CFD Research Corp., HTTP: http://www.cfdrc.com/

[19] Anderson, J.D. Jr., Modern Compressible Flow," 2nd ed., St. Louis: McGraw-Hill, 1990.

APPENDIX

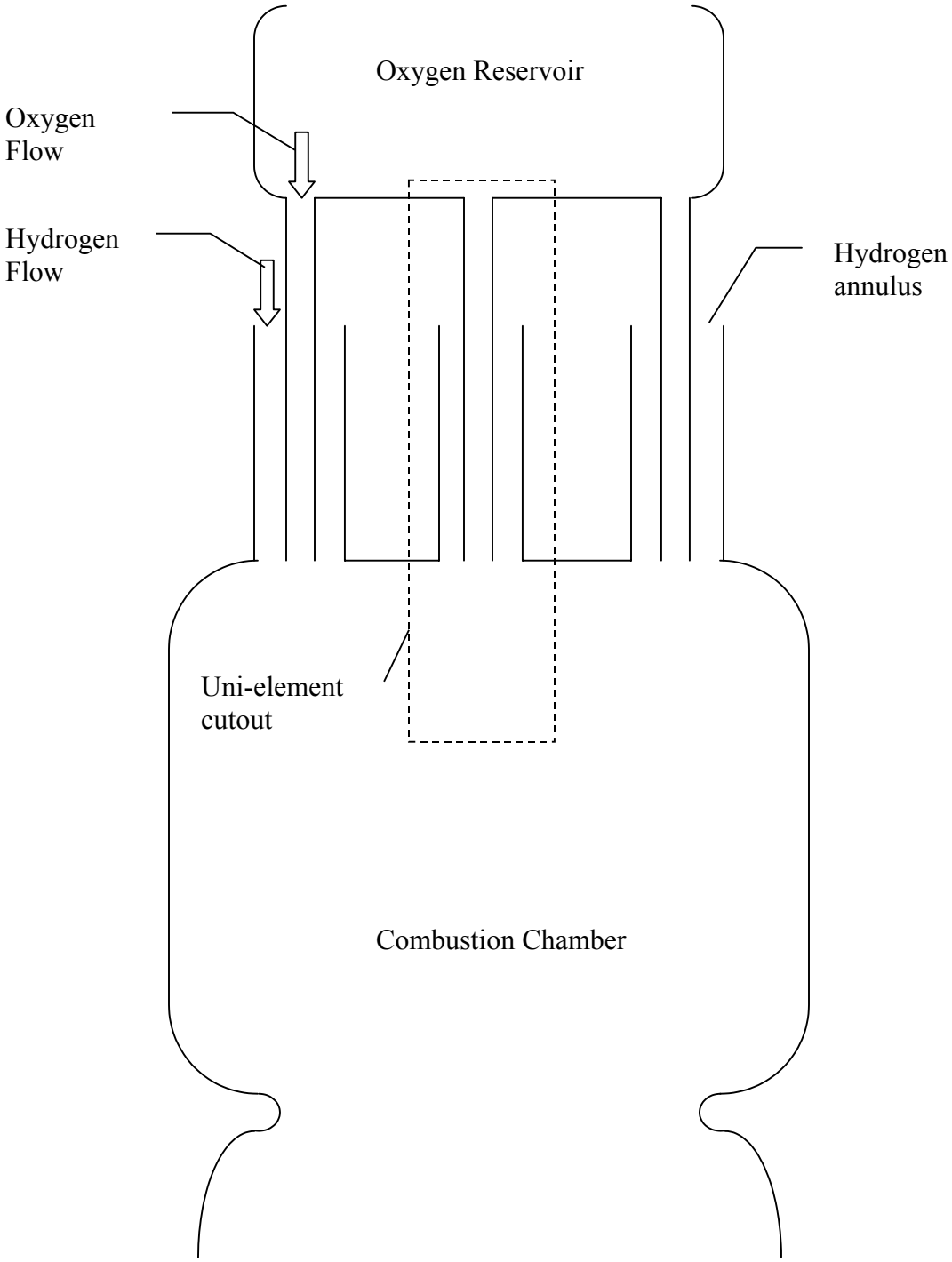

Figure 1: Shear Coaxial Injector Assembly

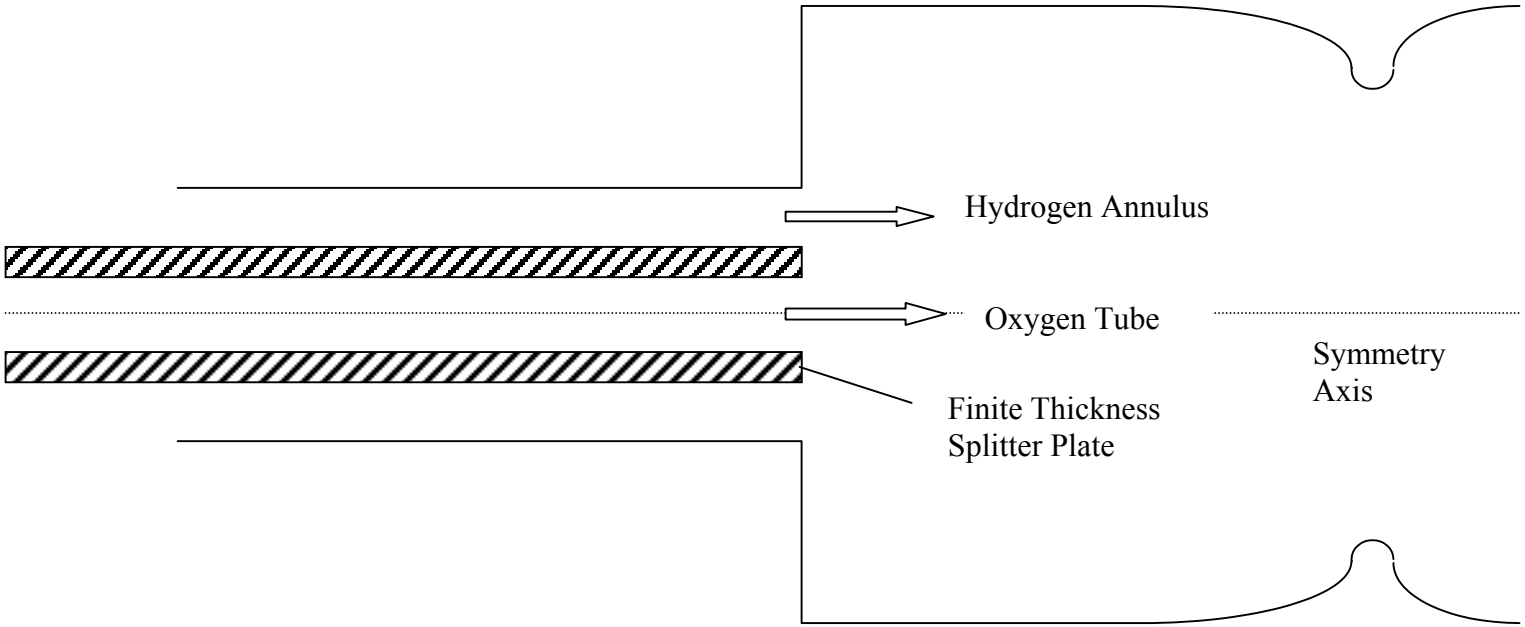

Figure 2: Uni-element Coaxial Injector

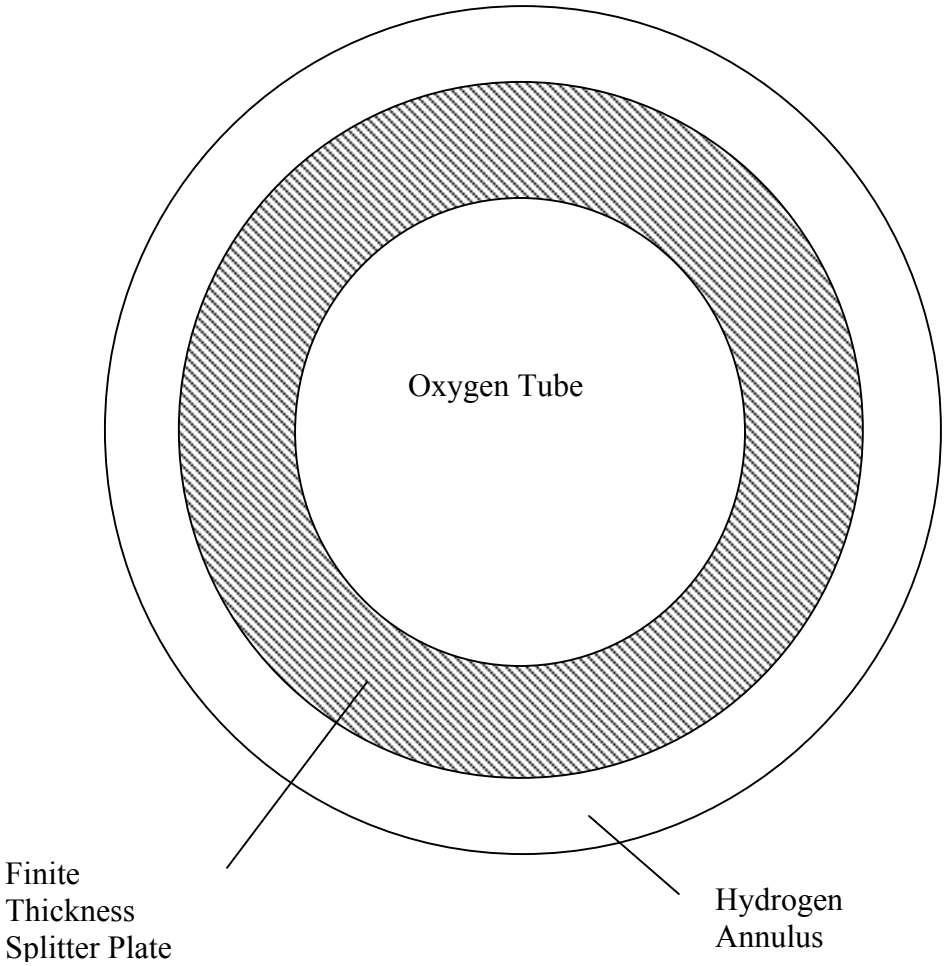

Figure 3: View Looking Down Coaxial Injector Tube

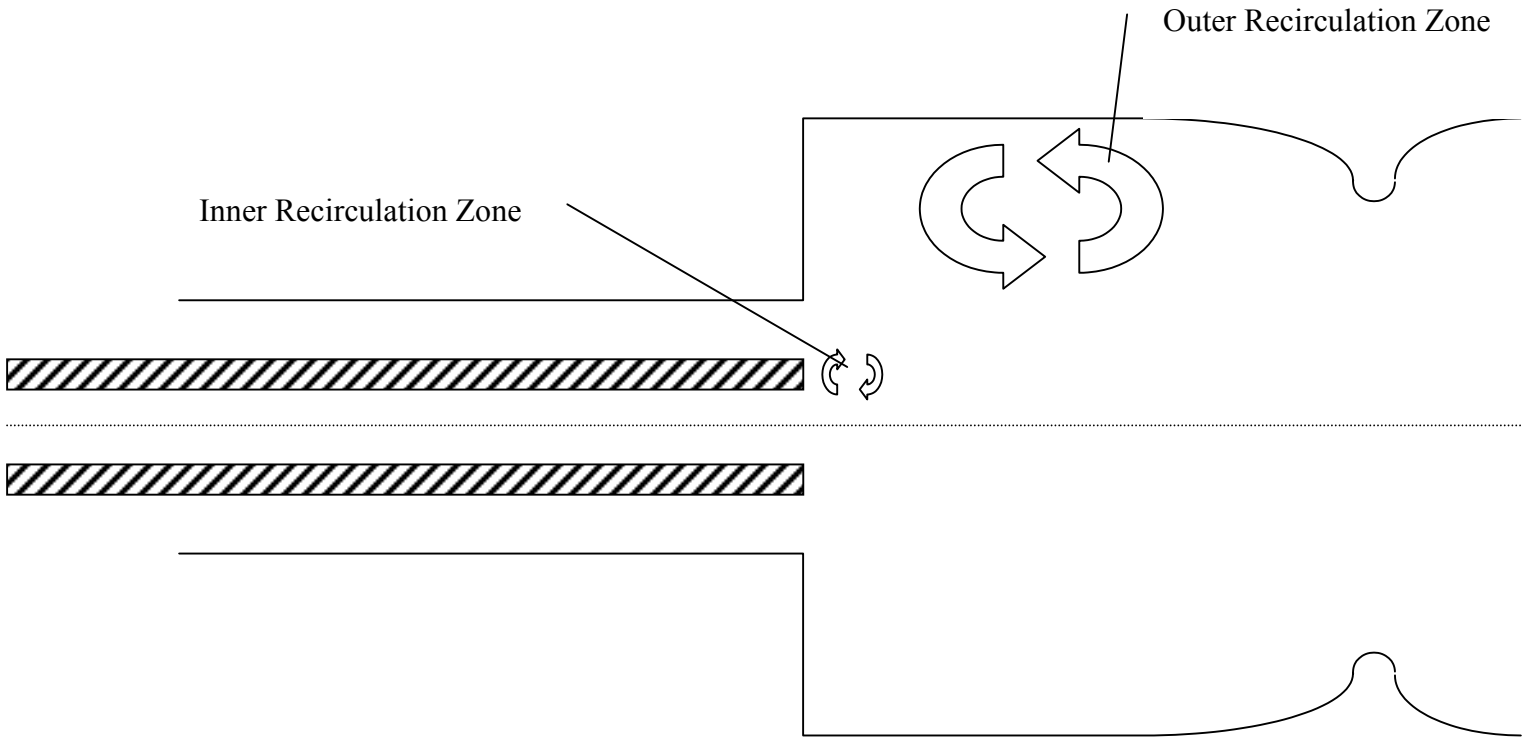

Figure 4: Circulation Regions

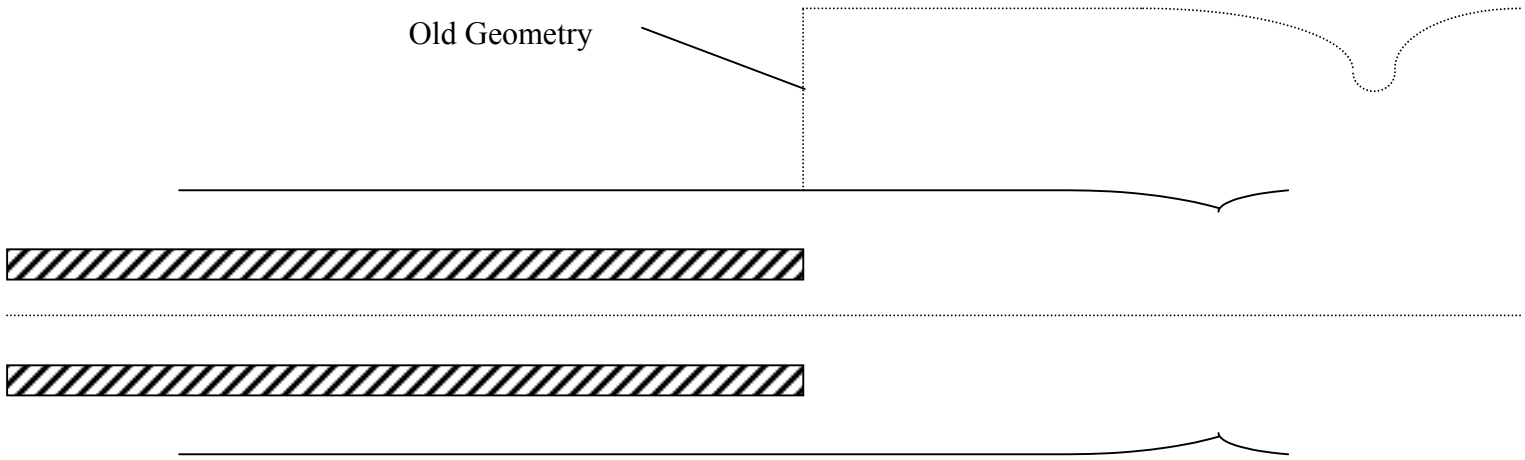

Figure 5: Combustion Chamber Cutoff

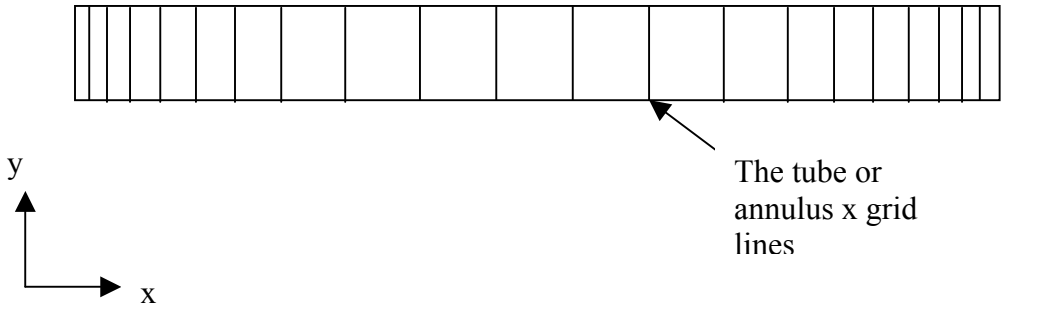

Fixed Δx

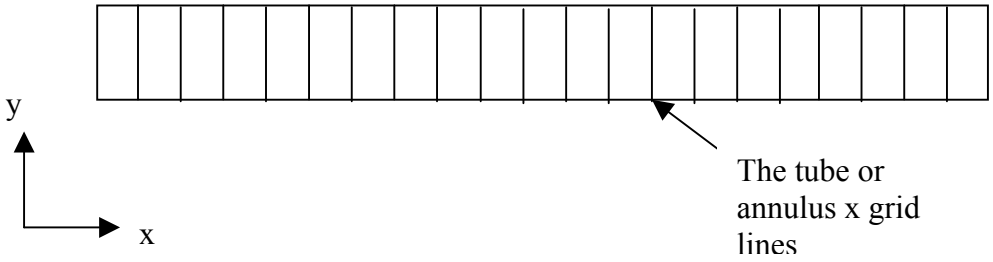

Figure 6: Stretching in the x Direction

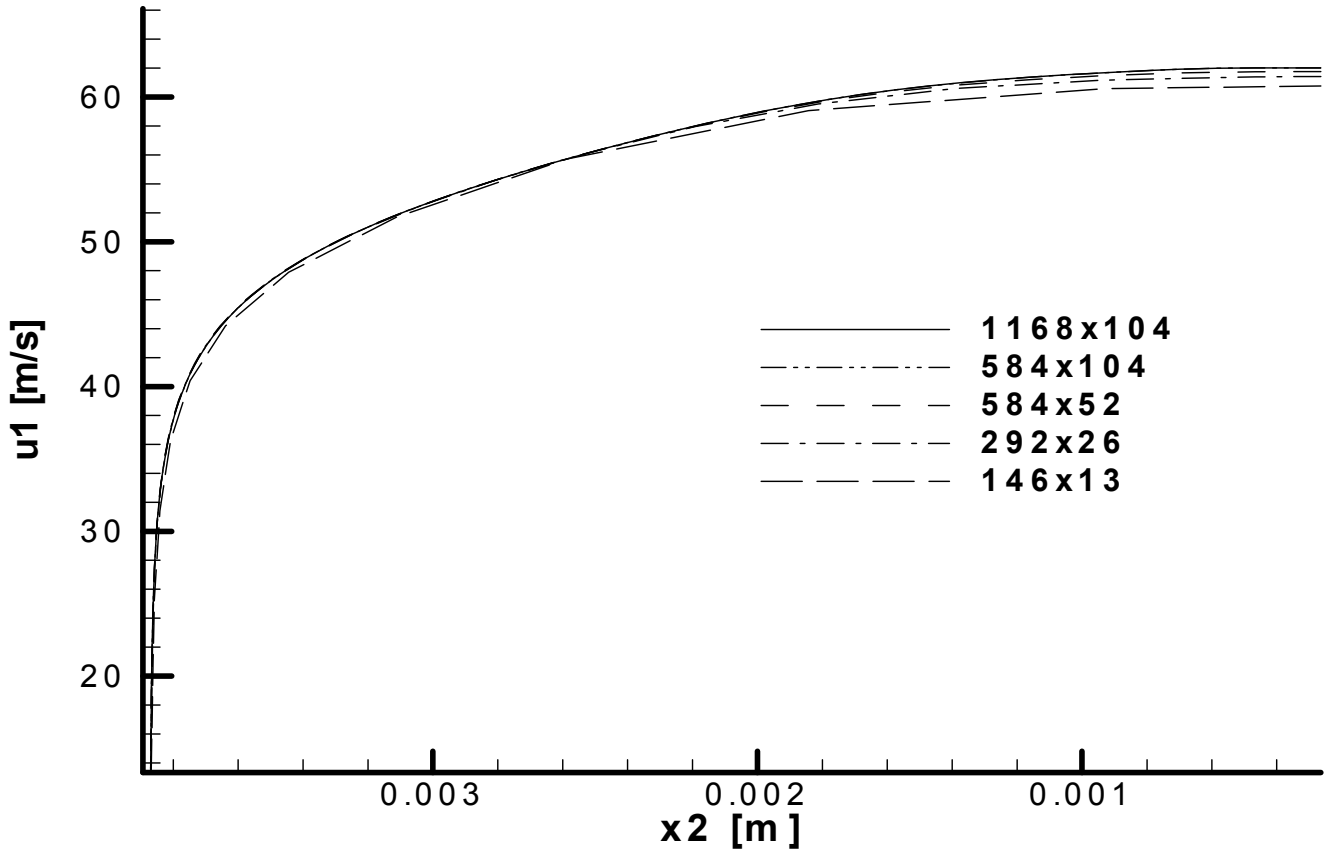

Figure 7: Oxygen Tube
Exit Velocity Profile Comparison

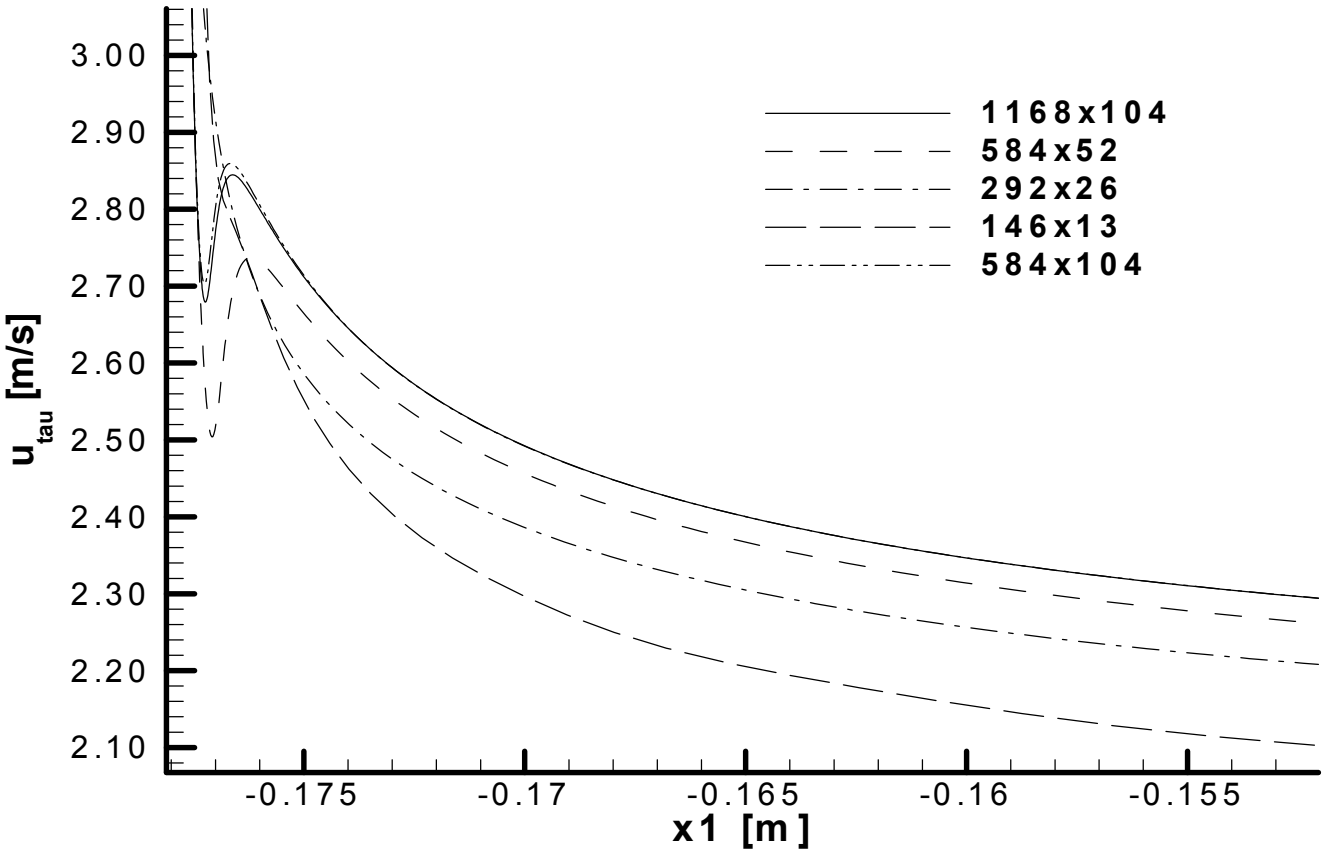

Figure 8: Oxygen Tube
Friction Velocity Comparison

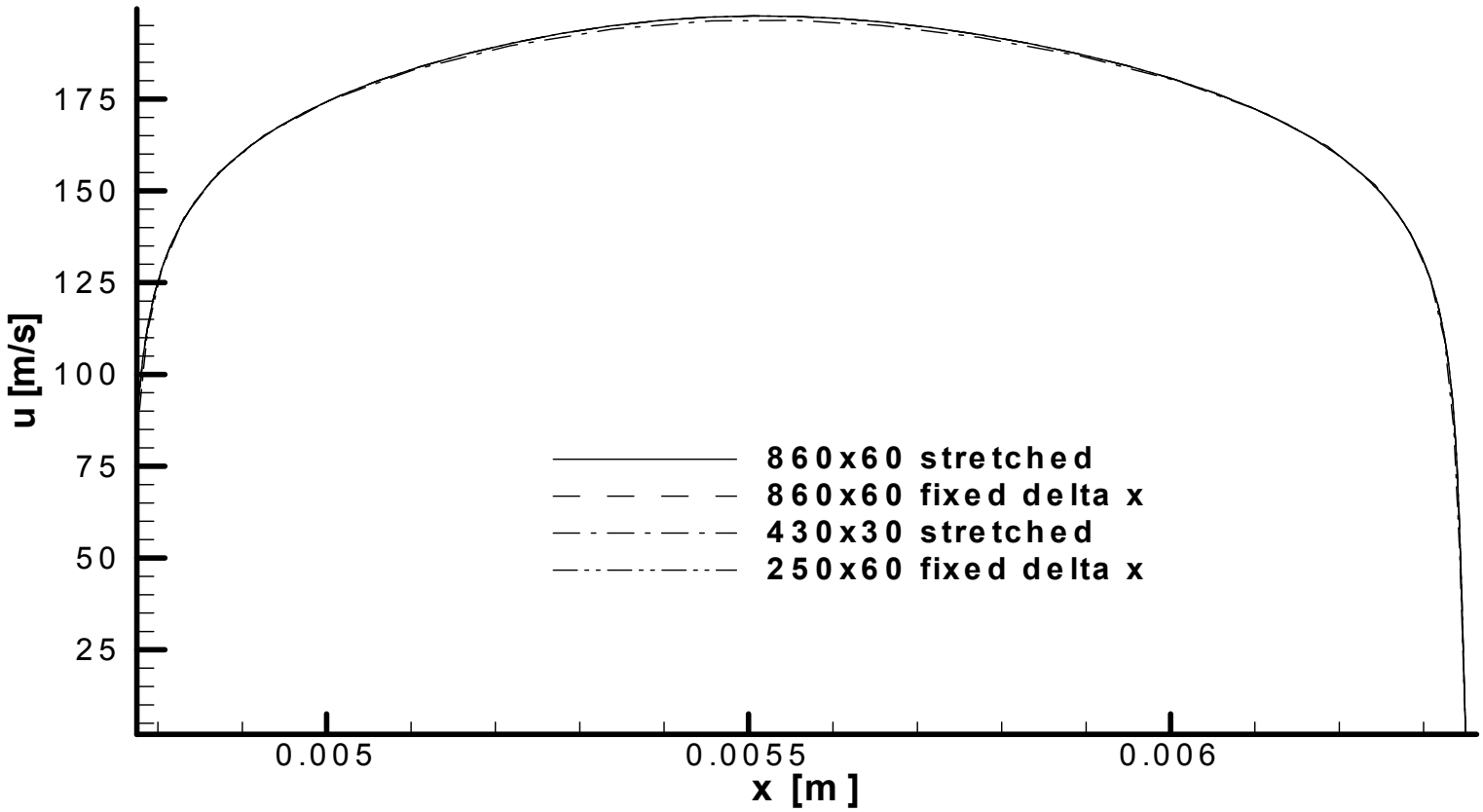

Figure 9: Hydrogen Annulus
Exit Velocity Profile Comparison

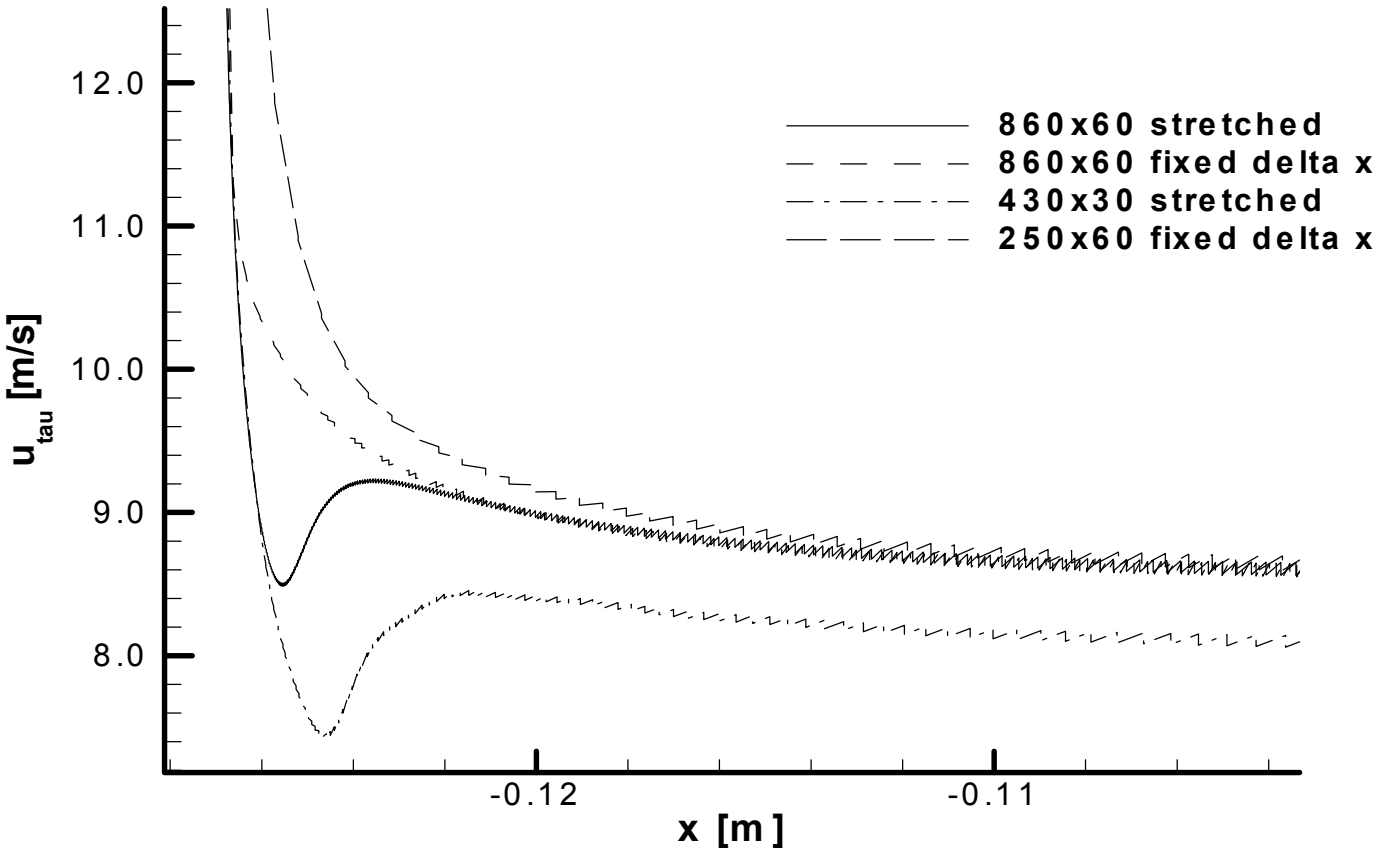

Figure 10: Hydrogen Annulus Friction Velocity Comparison

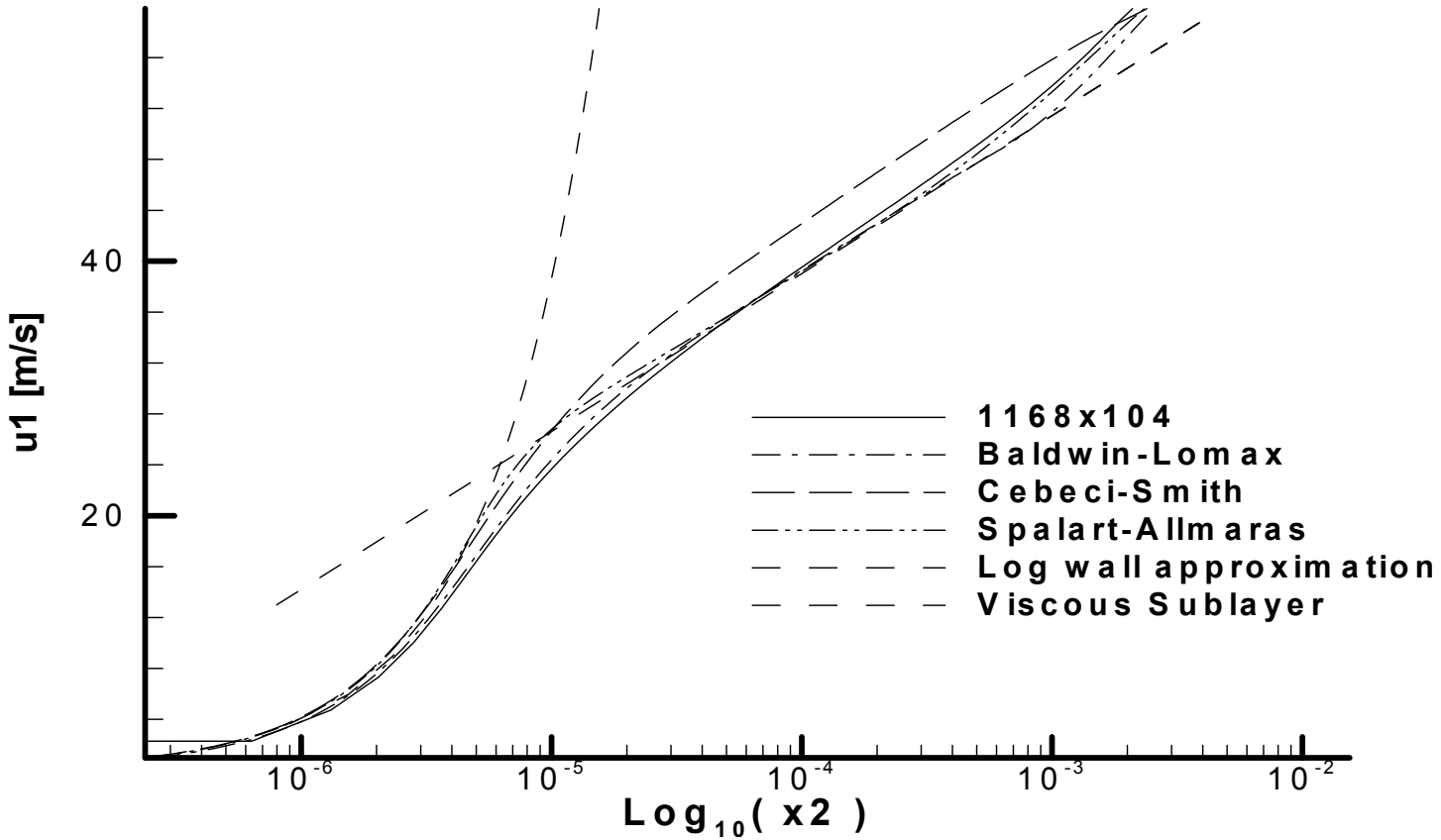

Figure 11: Oxygen Tube
Exit Velocity Profile Comparison Against Models

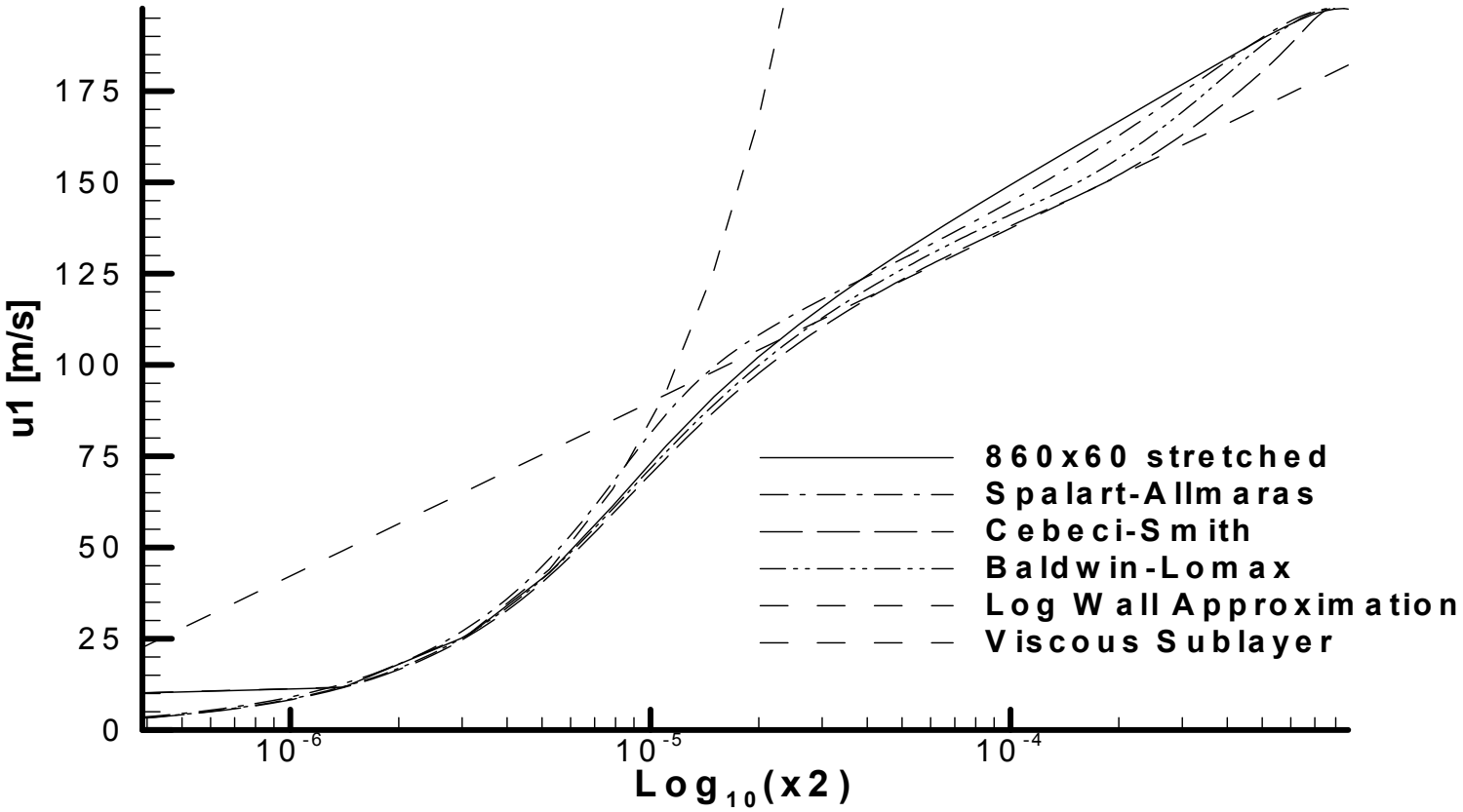

Figure 12: Hydrogen Annulus
Exit Velocity Profile Comparison Against Models

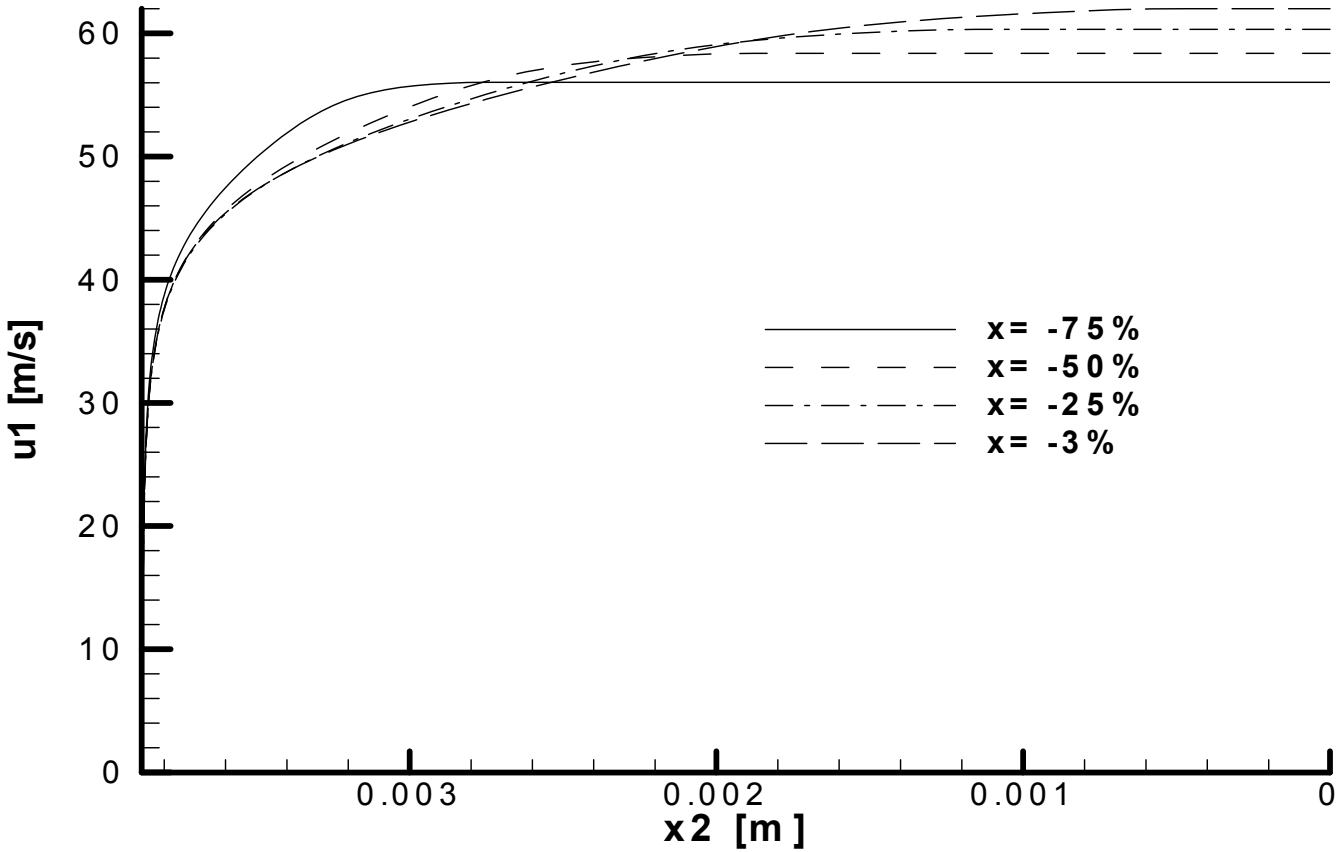

Figure 13: Development of Oxygen Velocity Profile on Stretched 1168x104 Grid

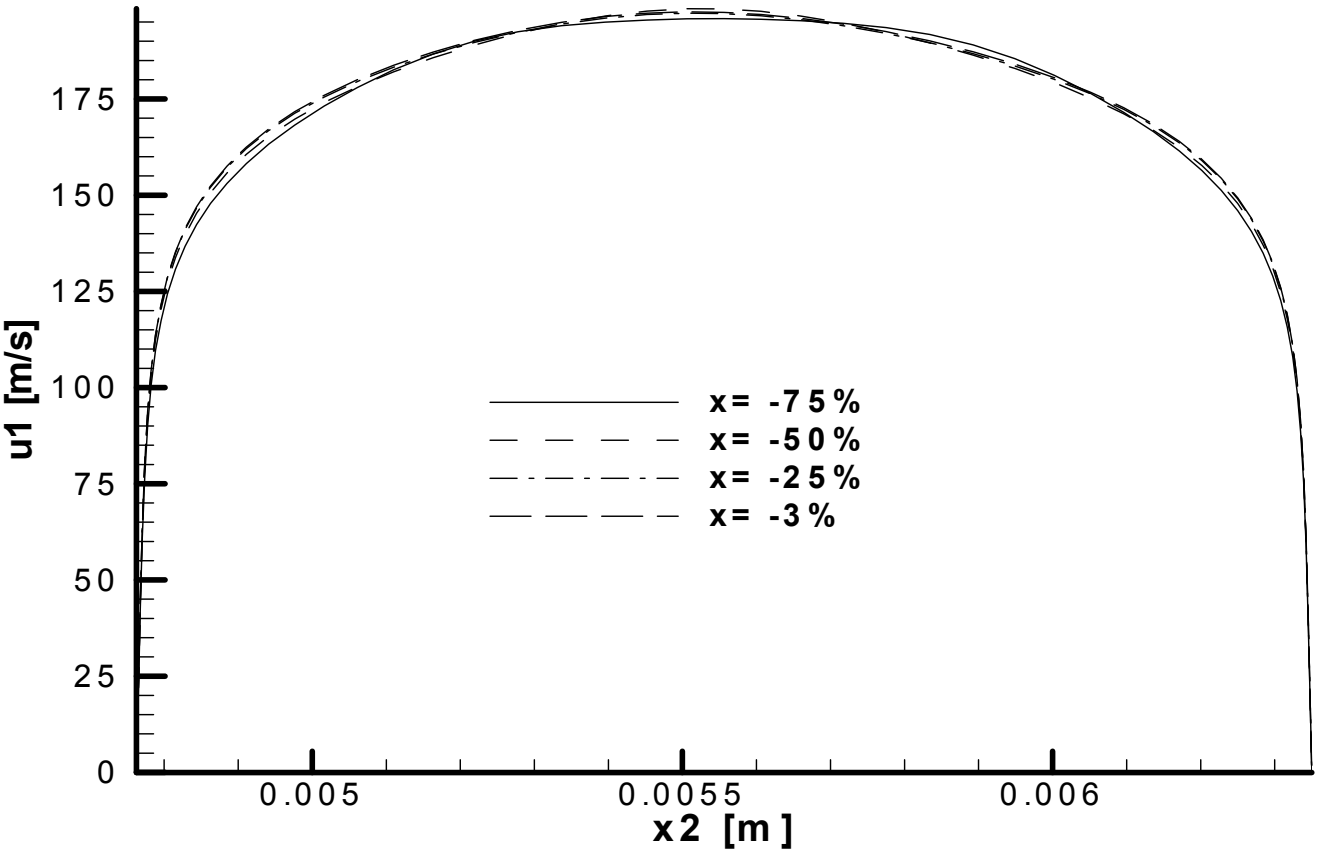

Figure 14: Development of Hydrogen Velocity Profile on Stretched 860x60 Grid

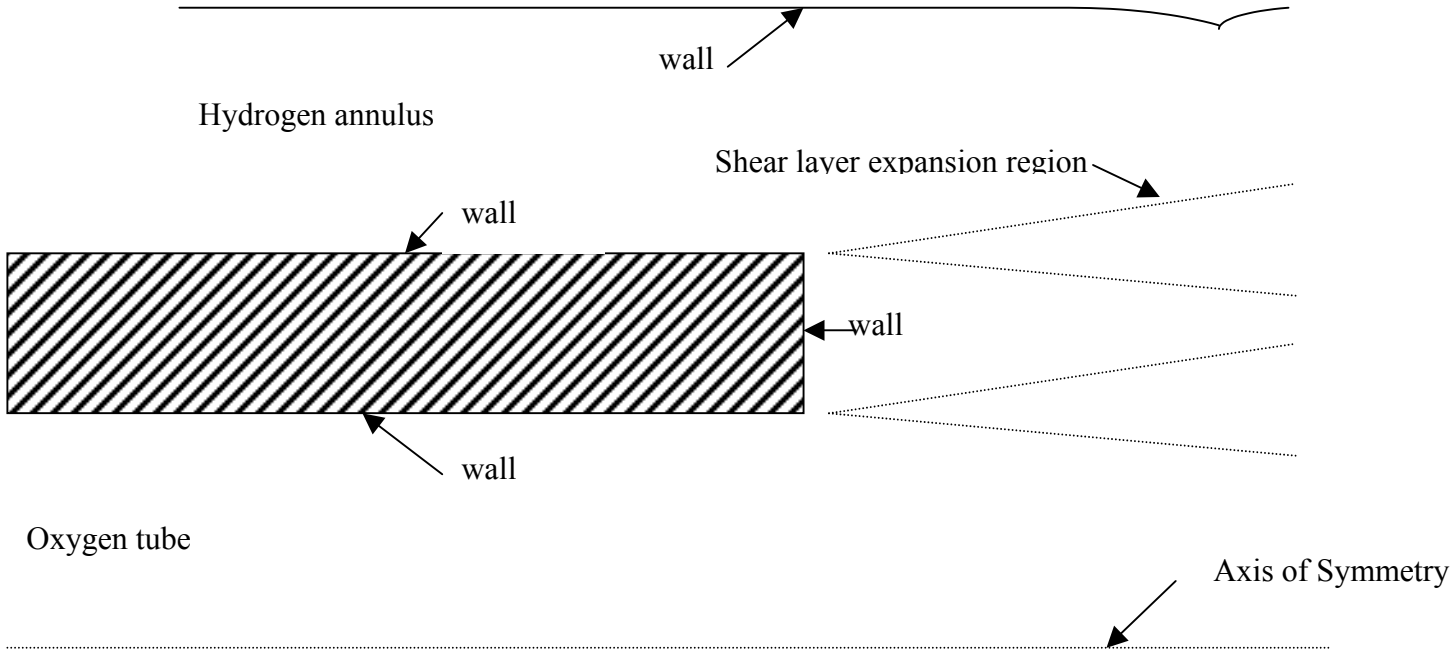

Figure 15: Grid Refinement Areas

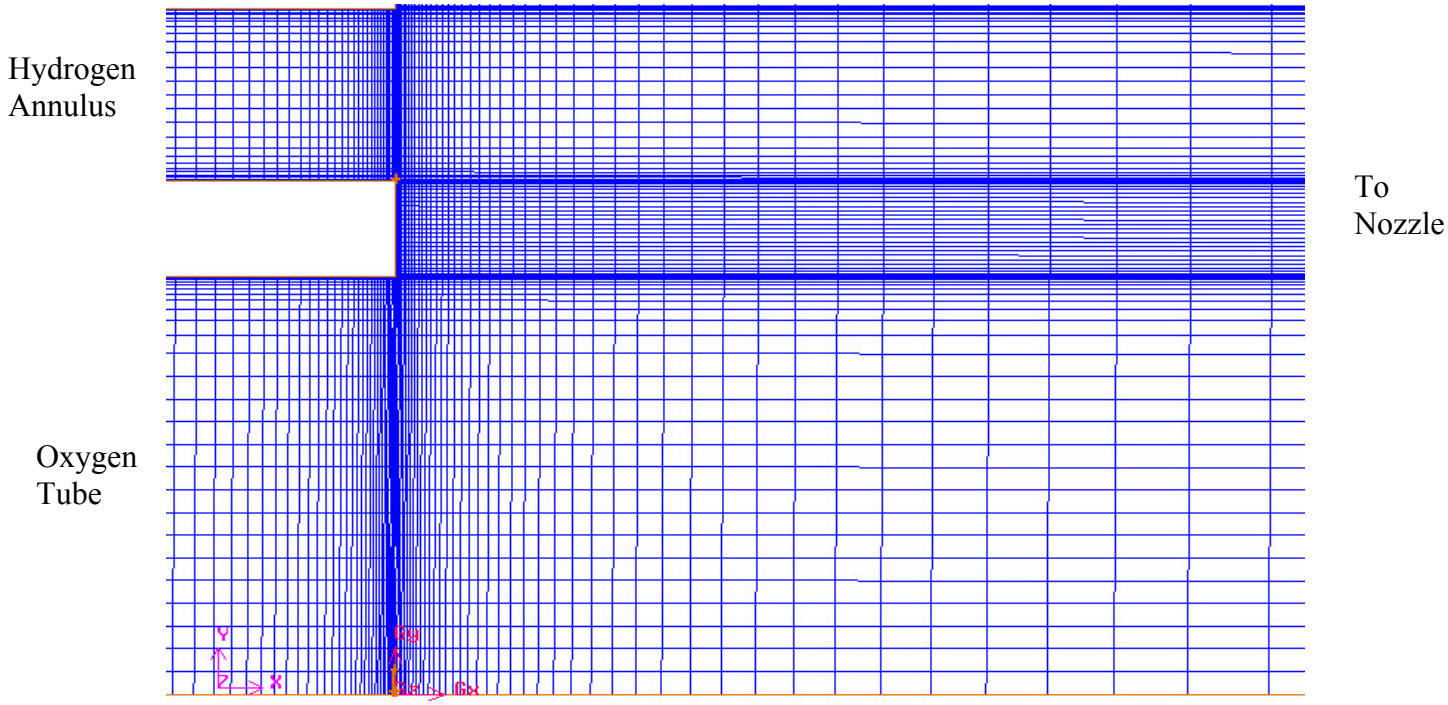

Figure 16: Inefficient Shear Layer Grid Scheme

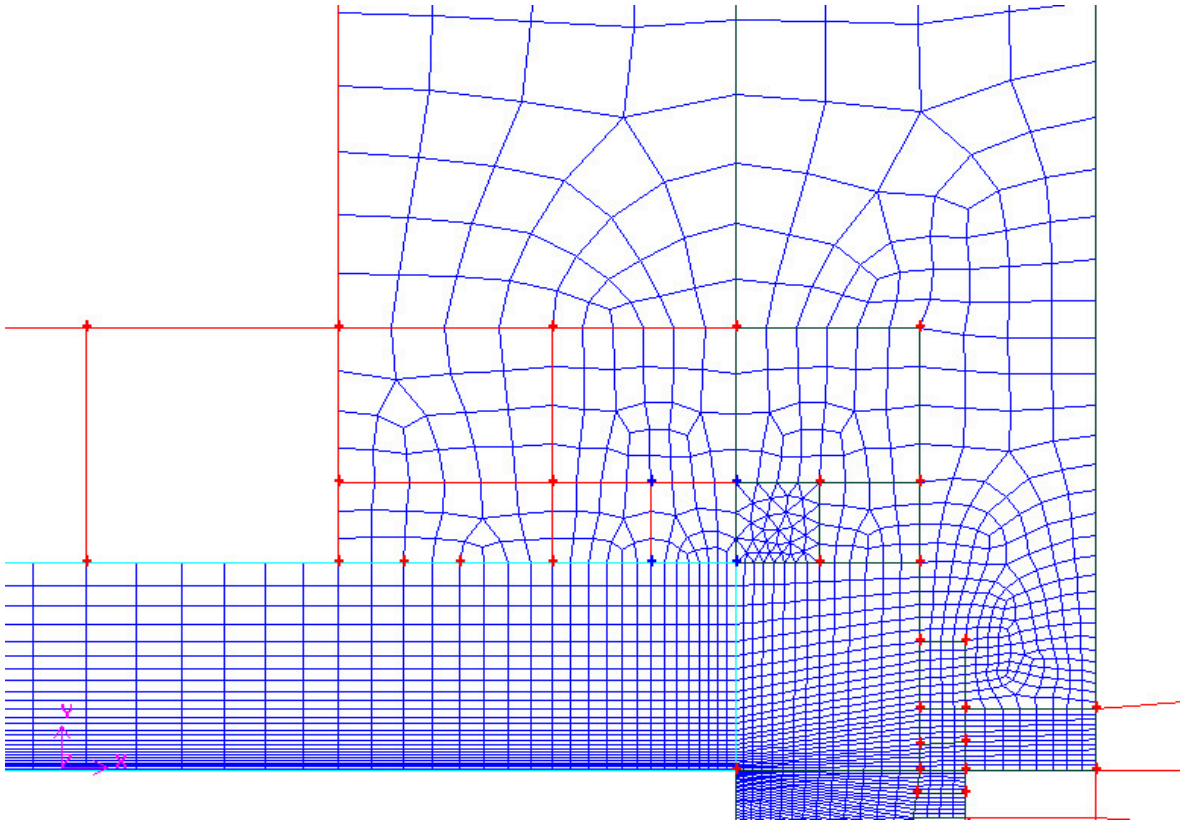

Figure 17: Visible Blocks of Grid Transitioning

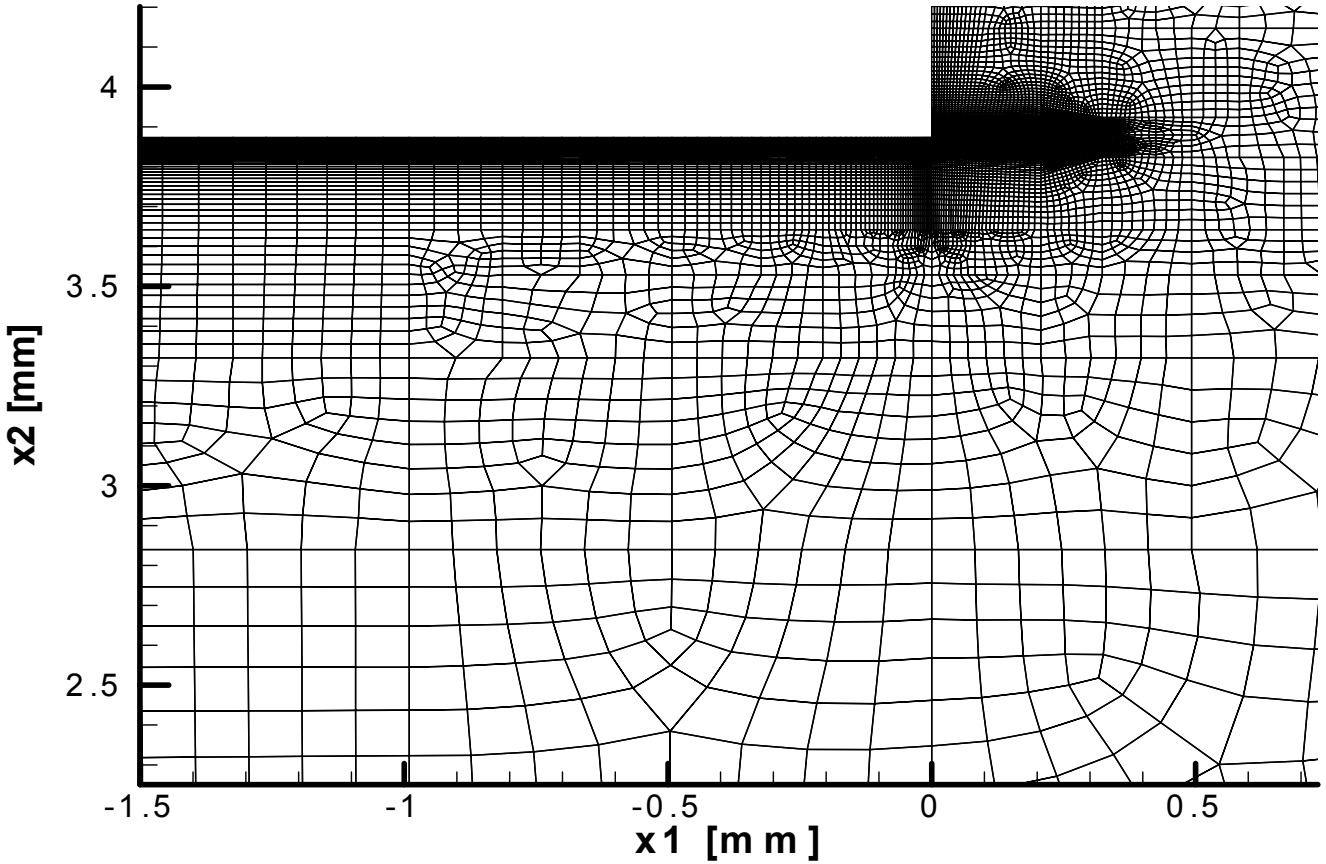

Figure 18: Oxygen Tube Grid Transitioning at Inlet/Chamber Interface

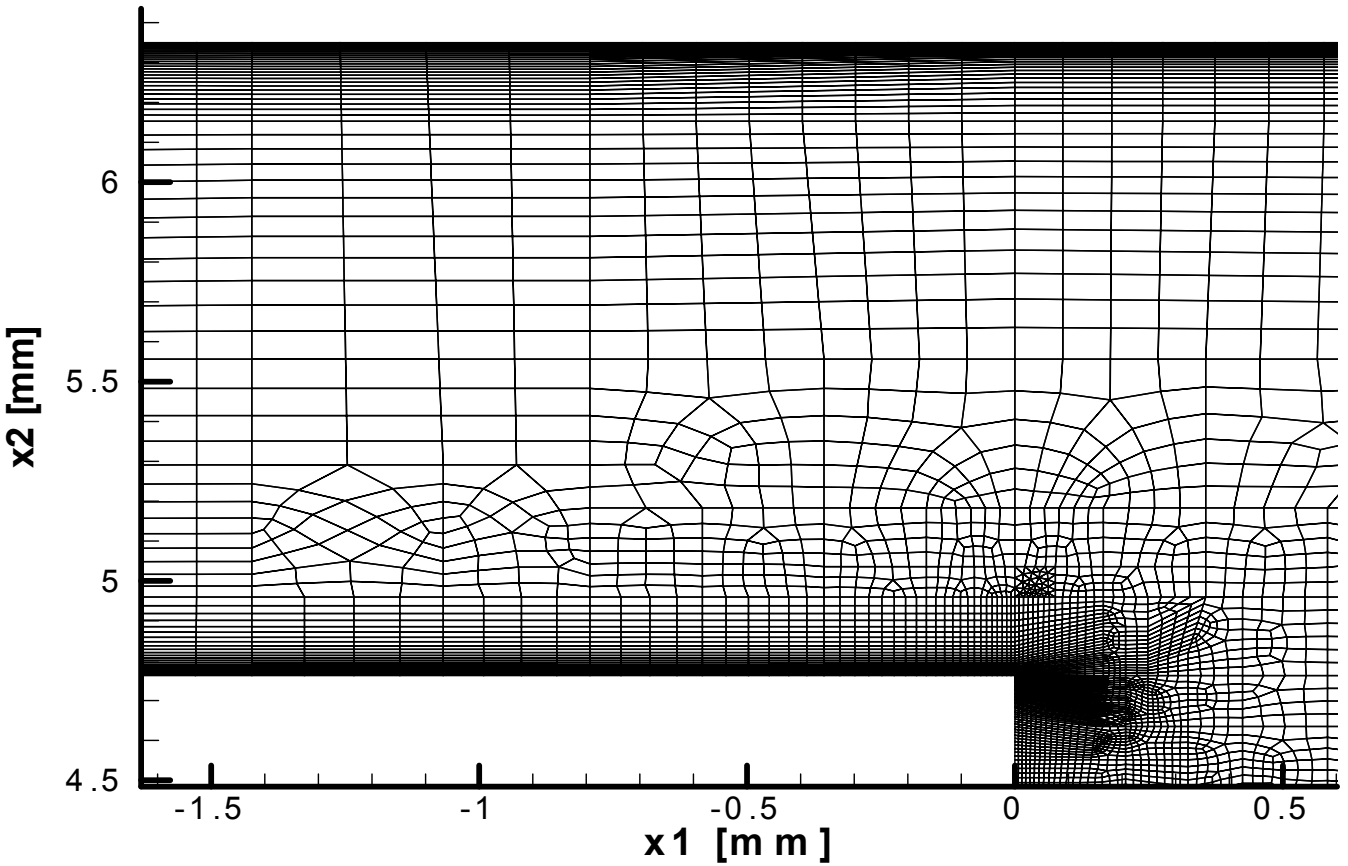

Figure 19: Hydrogen Annulus Grid Transitioning at Inlet/Chamber Interface

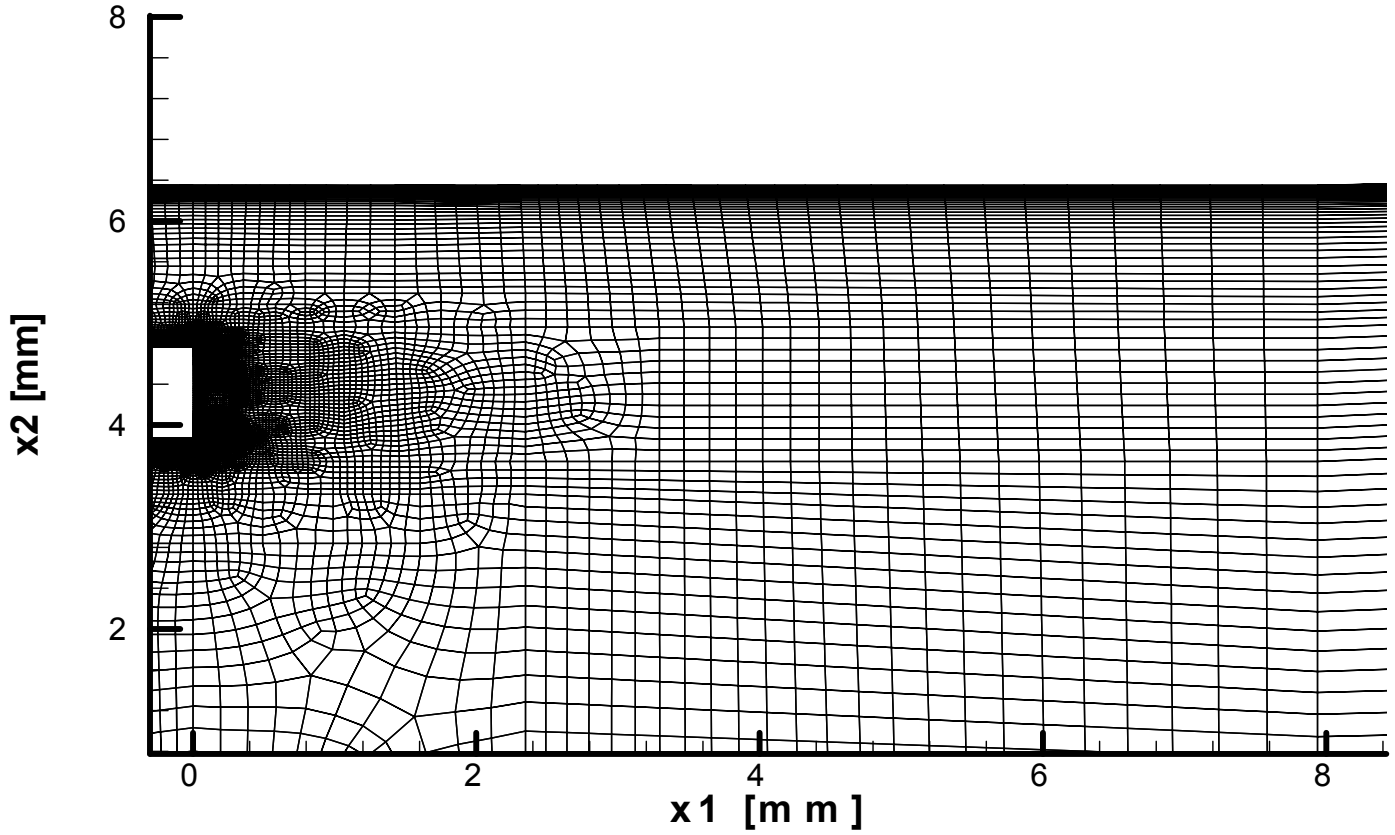

Figure 20: Shear Layer Coarse Grid

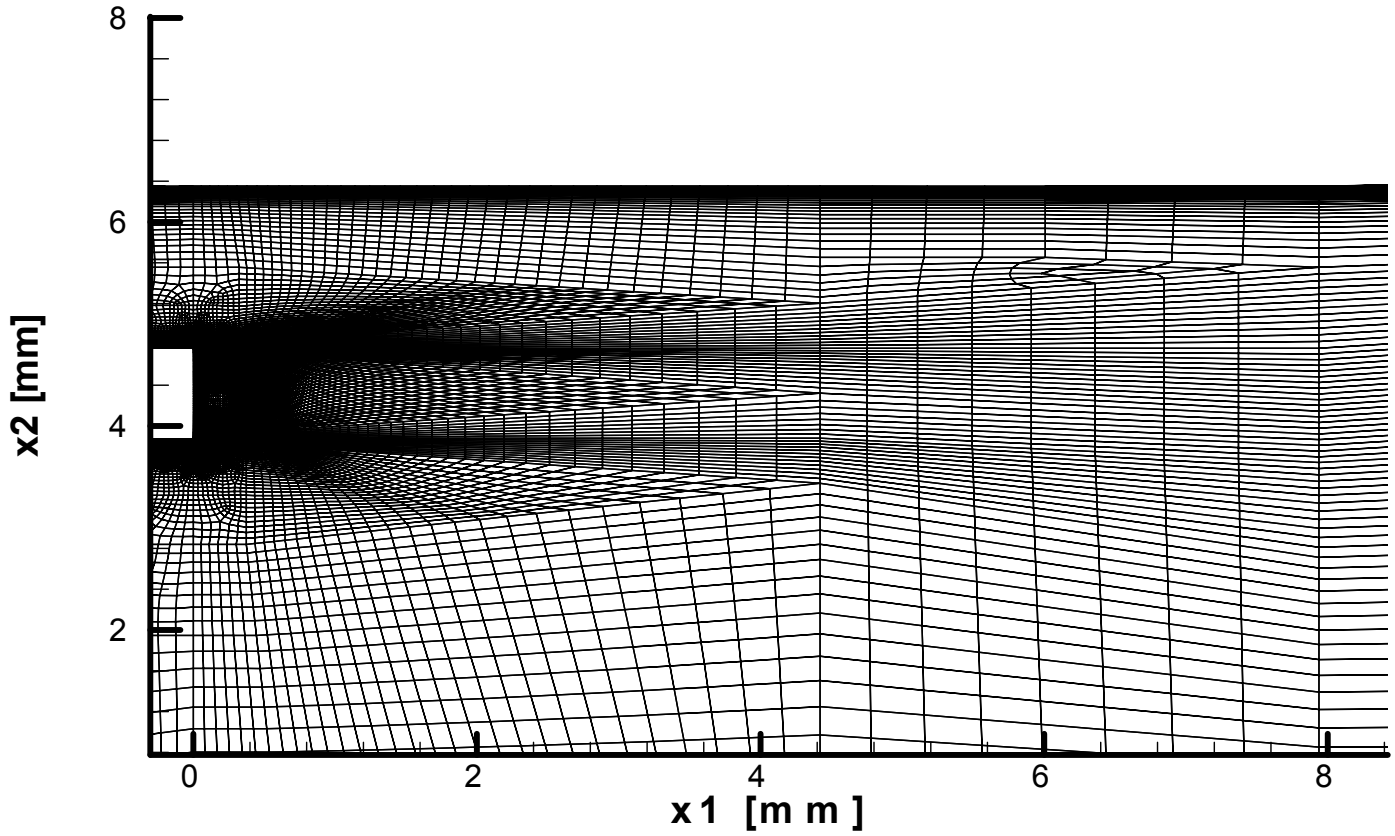

Figure 21: Shear Layer Refined Grid

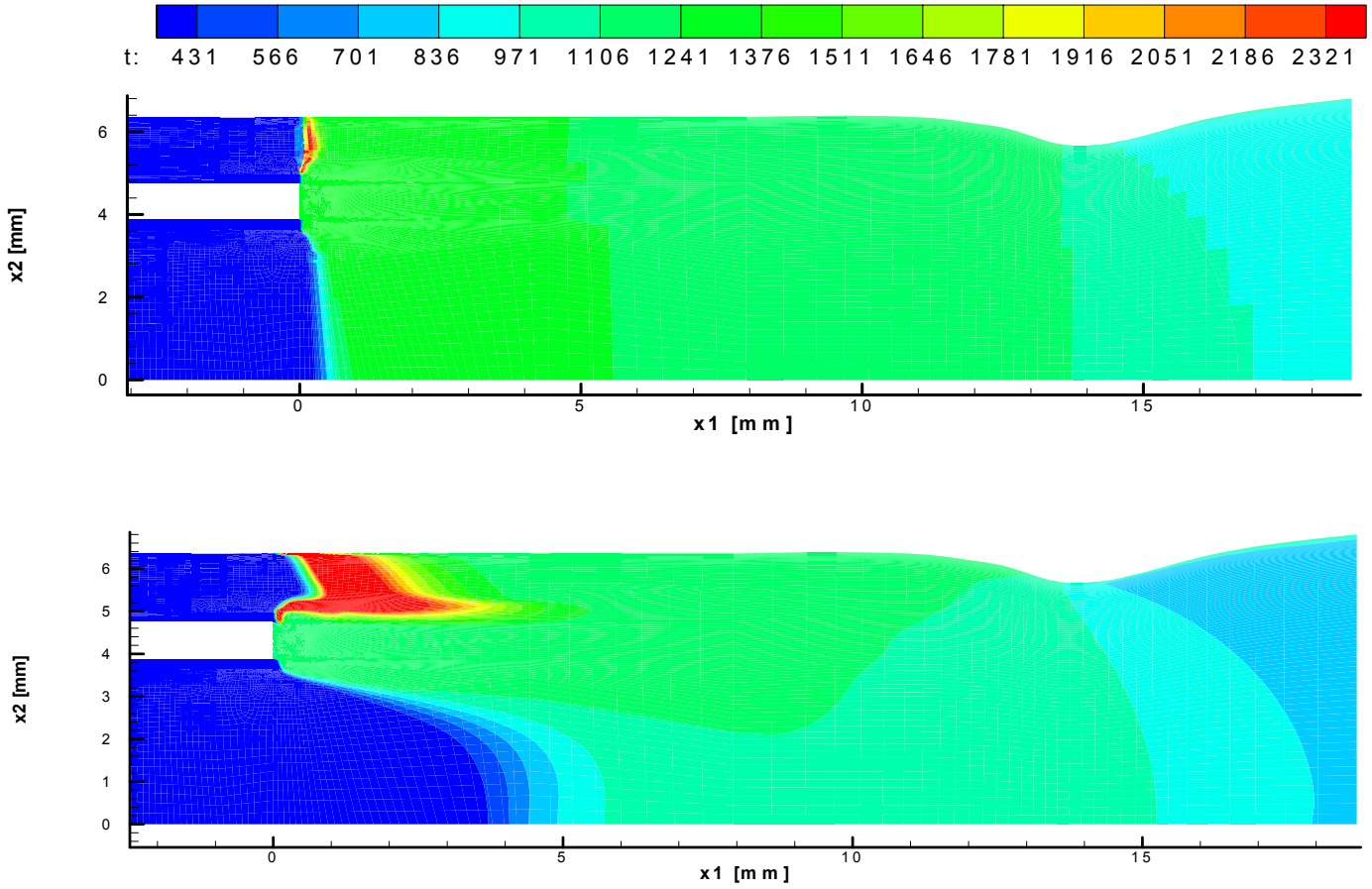

Figure 22: Temperature Contour During Ignition of Flame

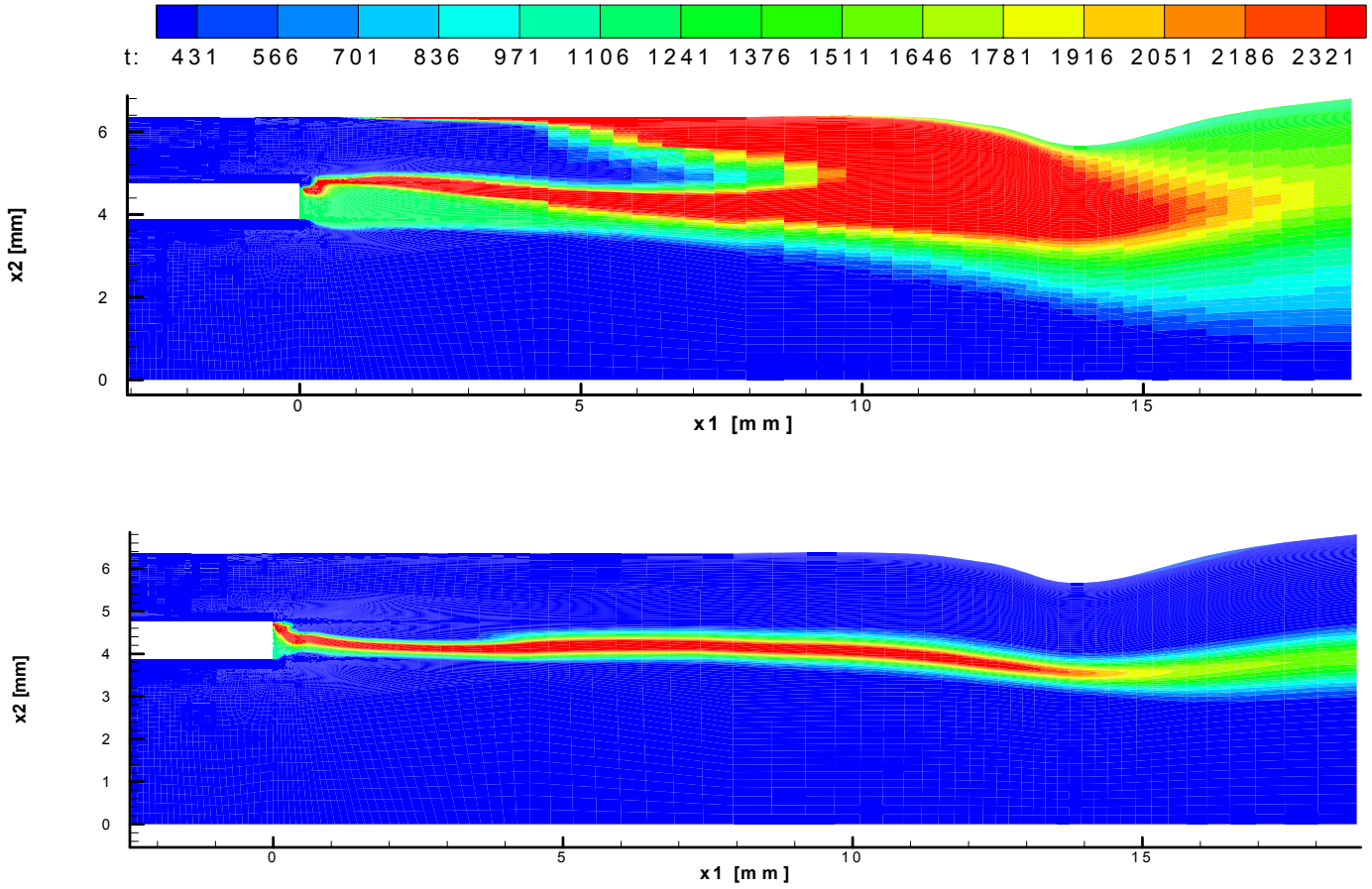

Figure 23: Temperature Contour As Flame Stabilizes

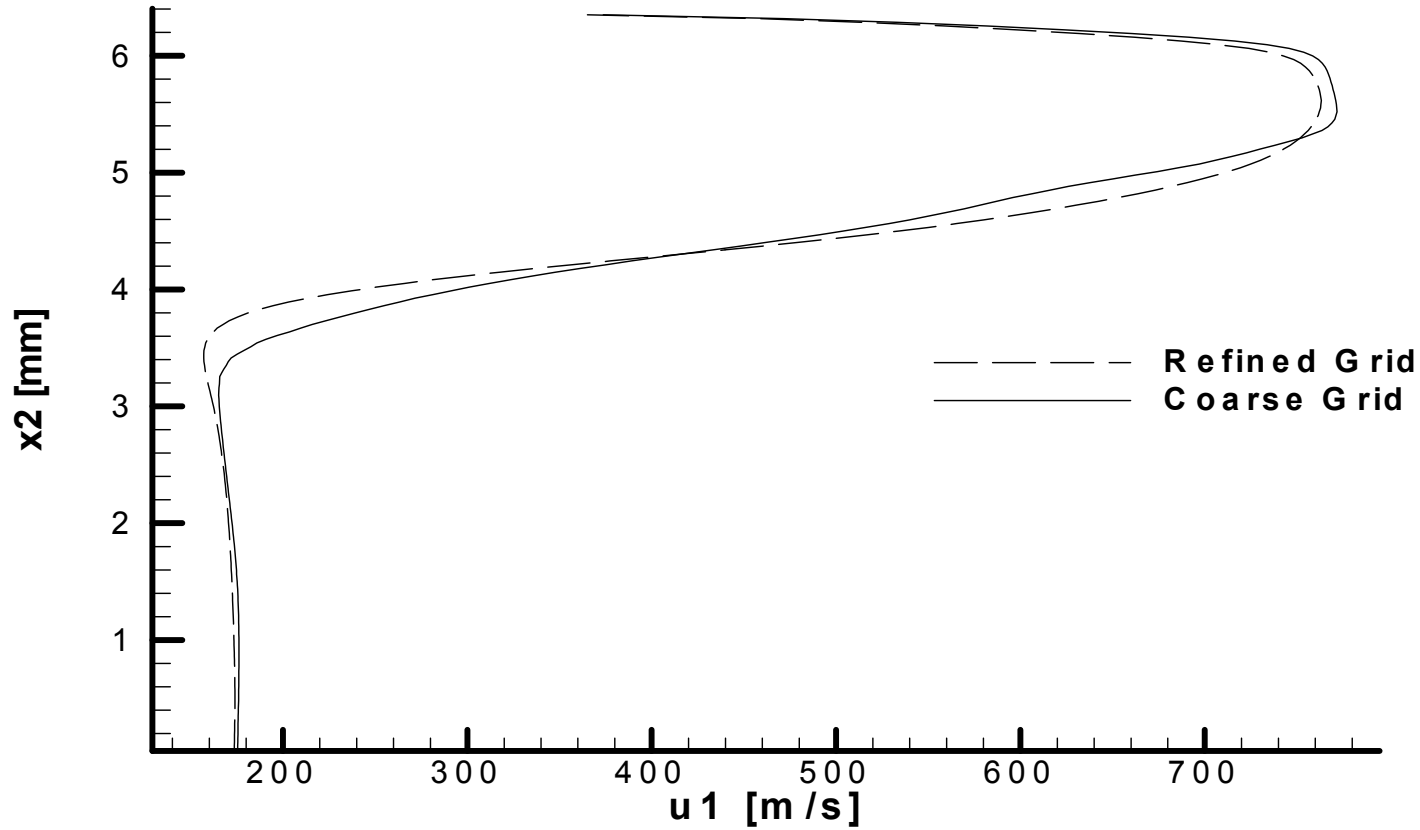

Figure 24: Velocity Profile Comparison in Chamber

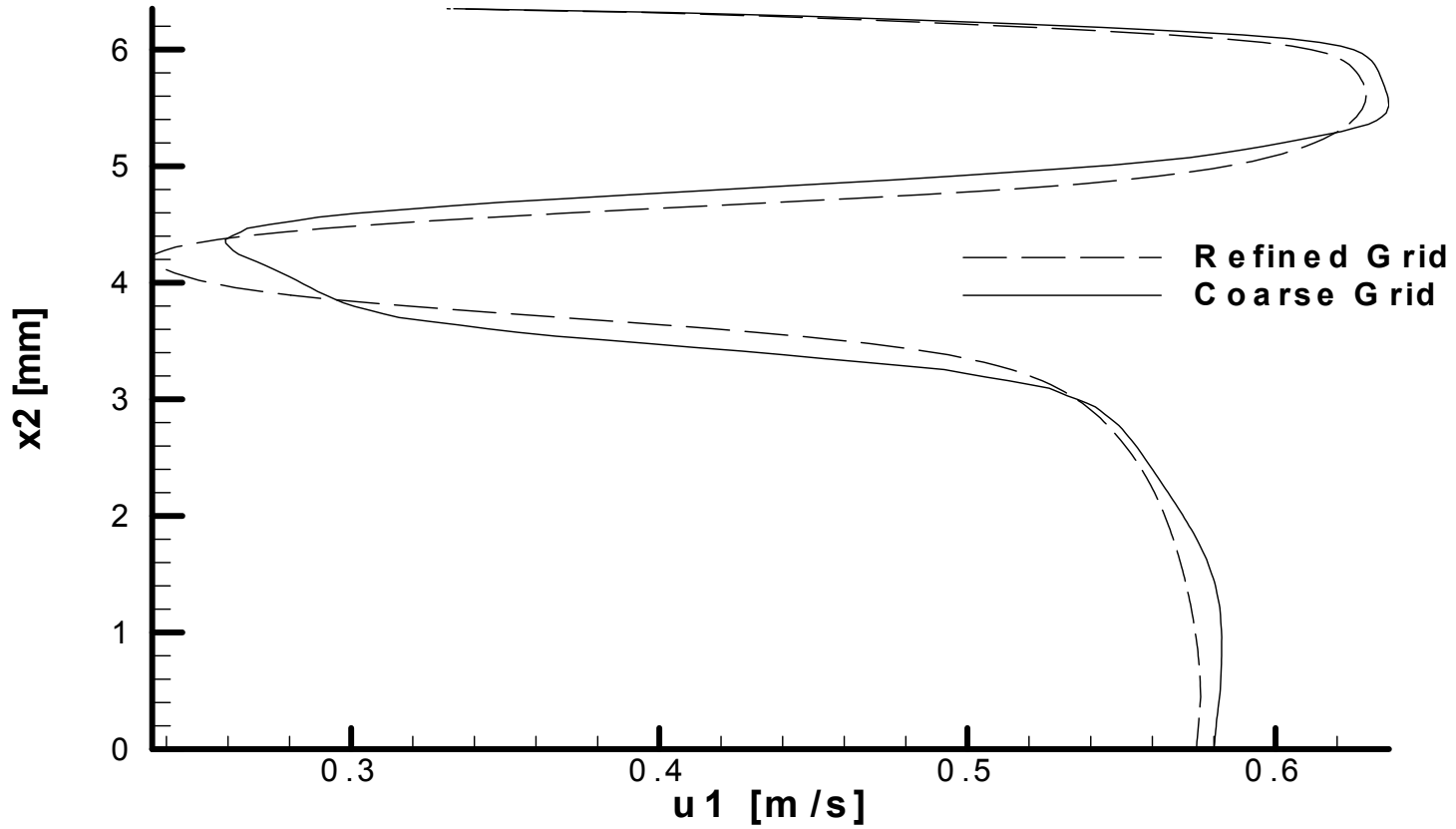

Figure 25: Mach Profile Comparison in Chamber

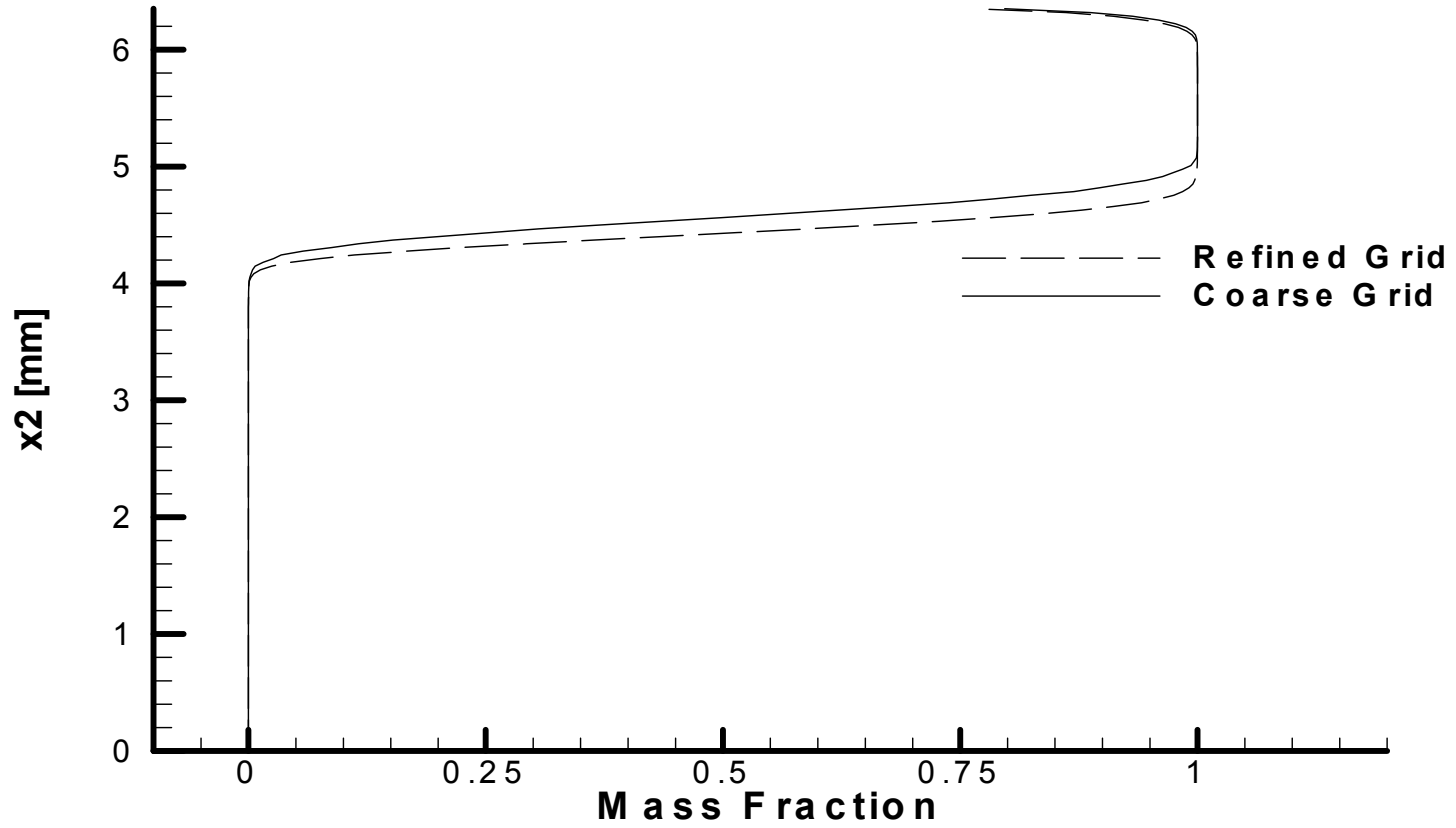

Figure 26: H_2 Profile Comparison in Chamber

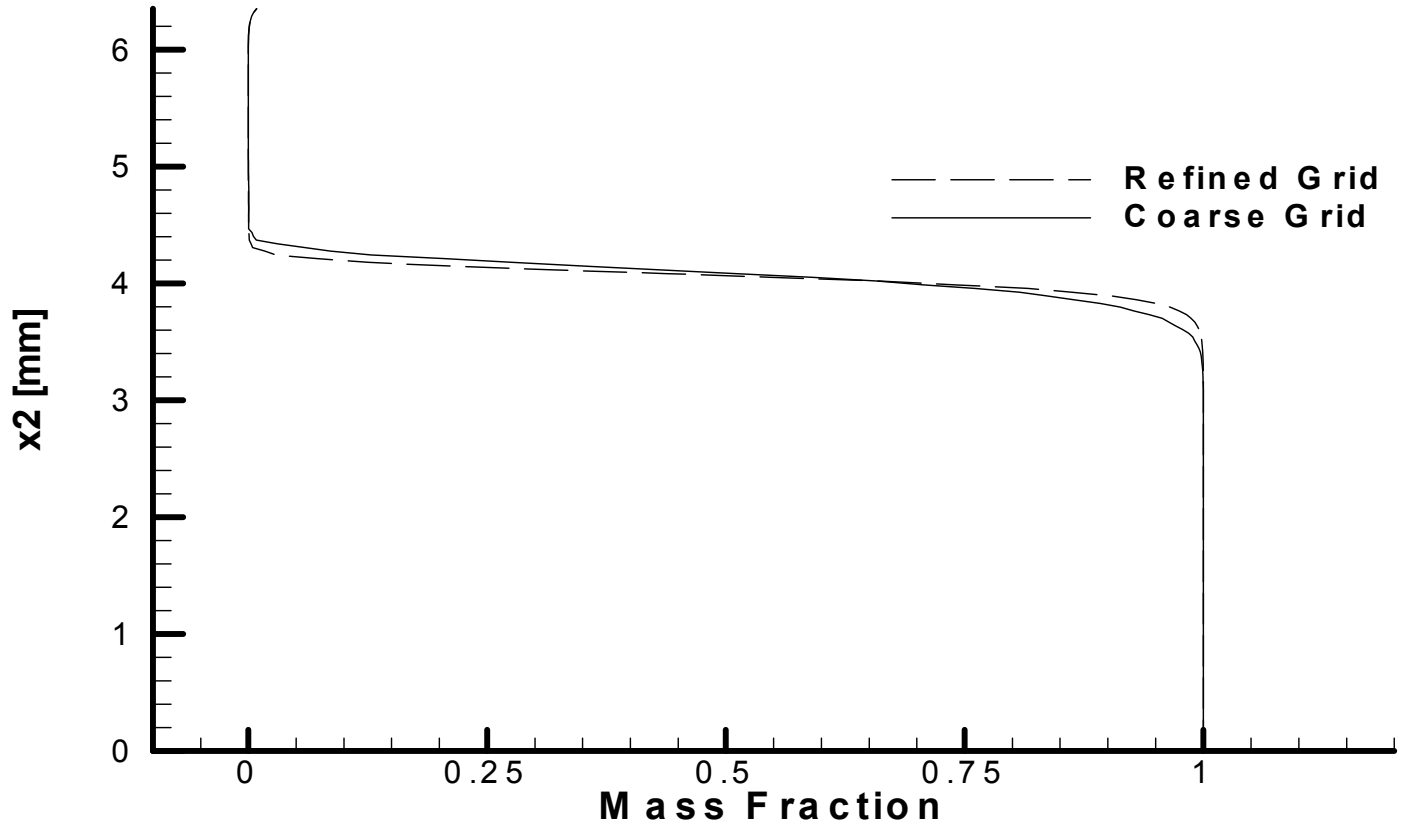

Figure 27: O_2 Profile Comparison in Chamber

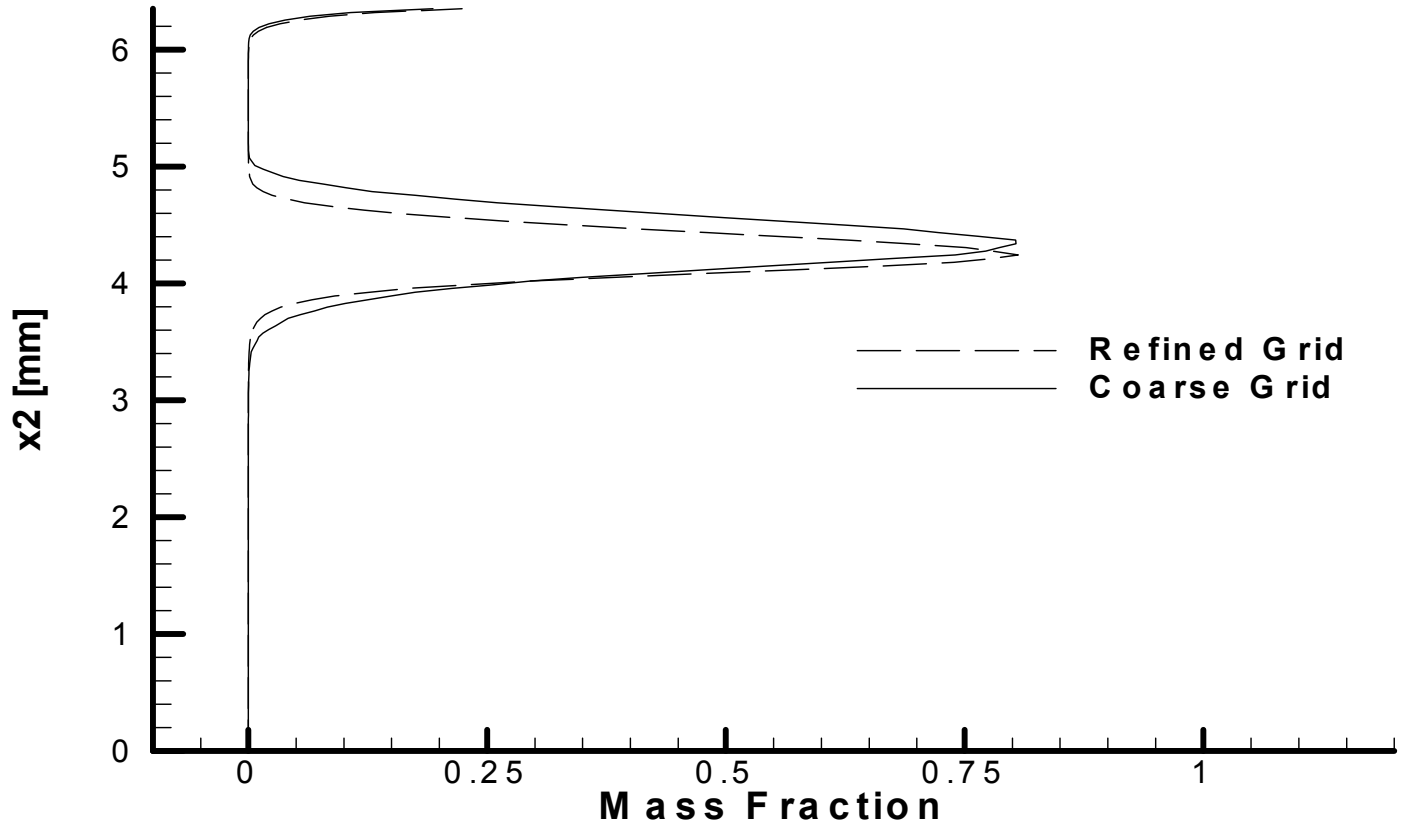

Figure 28: H_20 Profile Comparison in Chamber

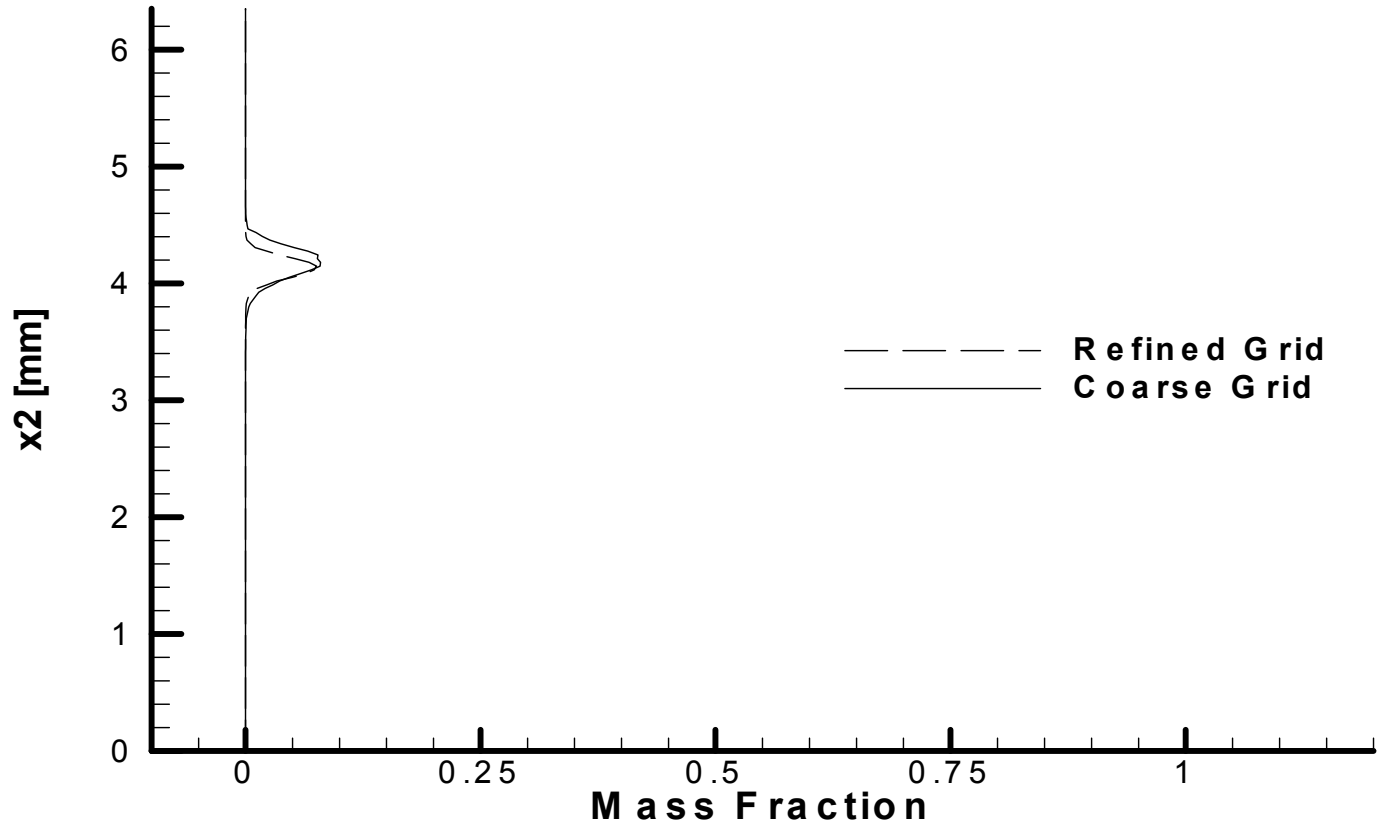

Figure 29: OH Profile Comparison in Chamber

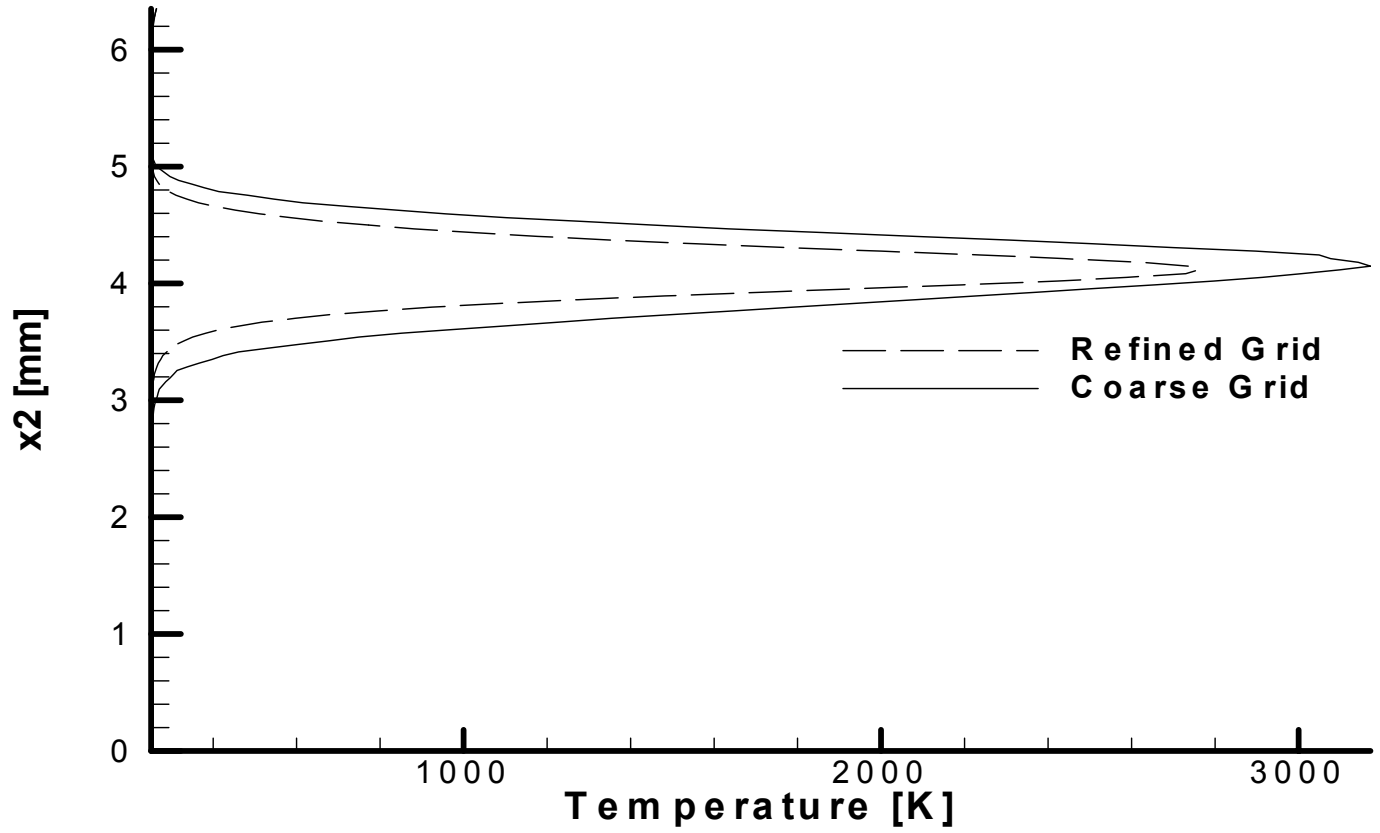

Figure 30: Temperature Profile Comparison in Chamber

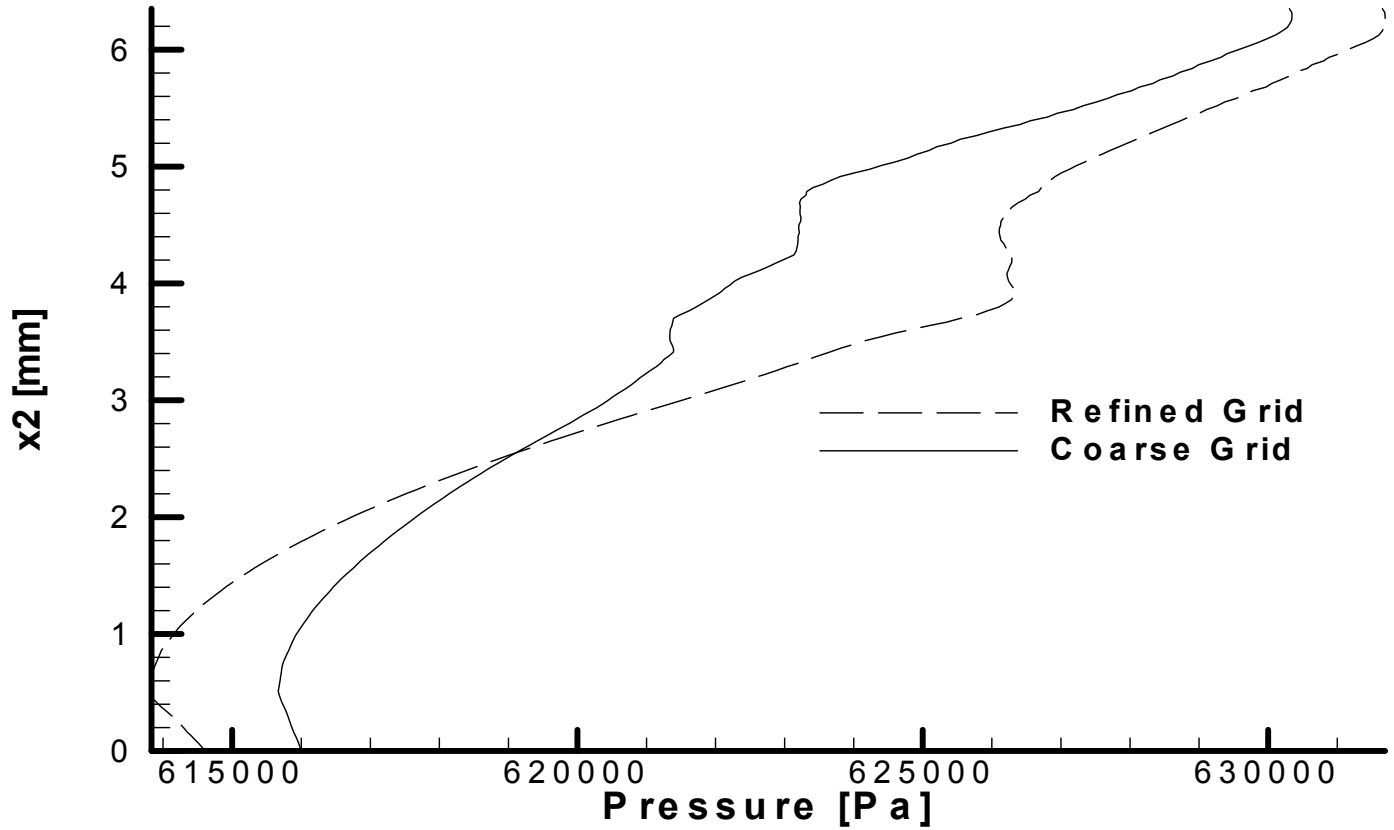

Figure 31: Pressure Profile Comparison in Chamber

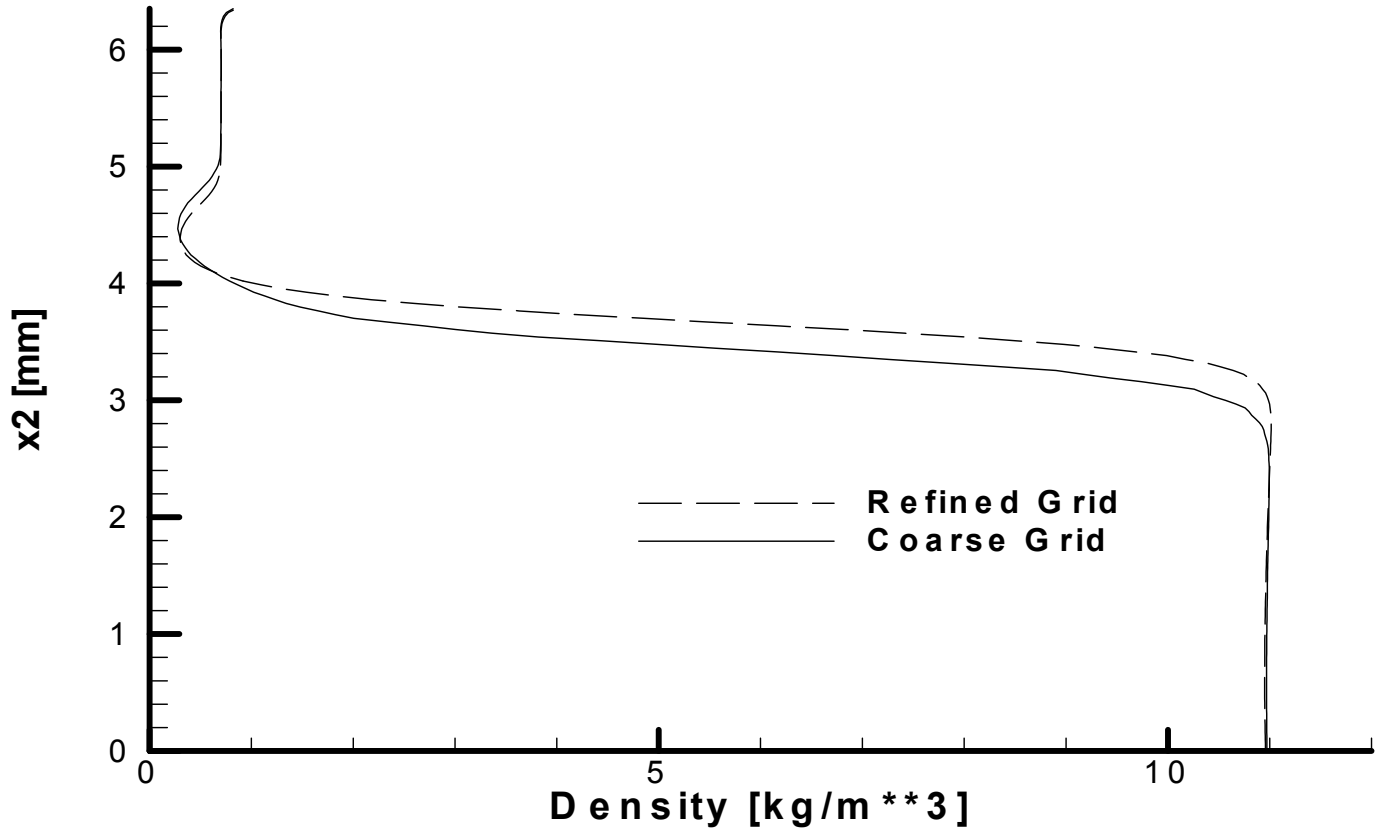

Figure 32: Density Profile Comparison in Chamber

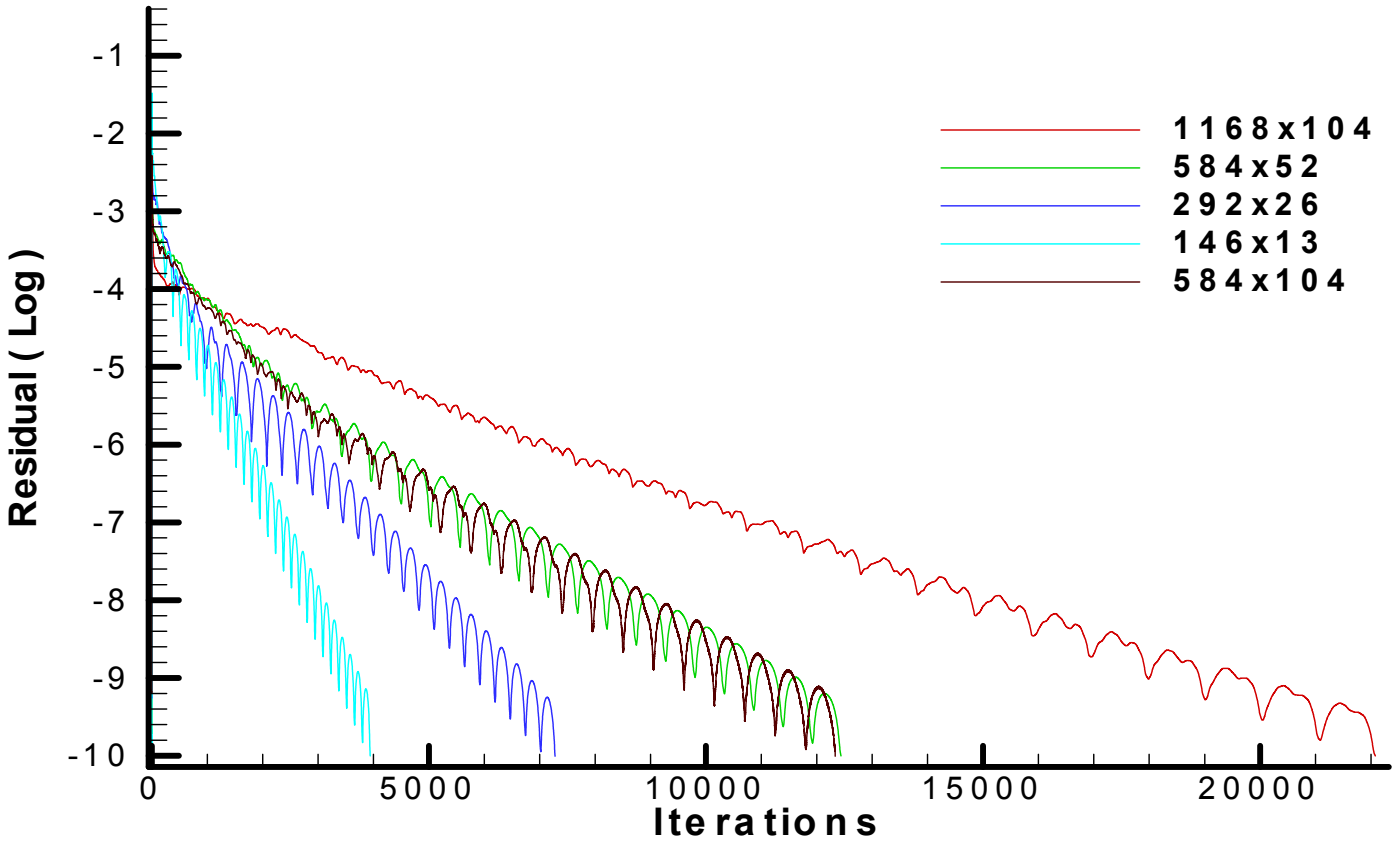

Figure 33: Oxygen Tube Convergence Comparison

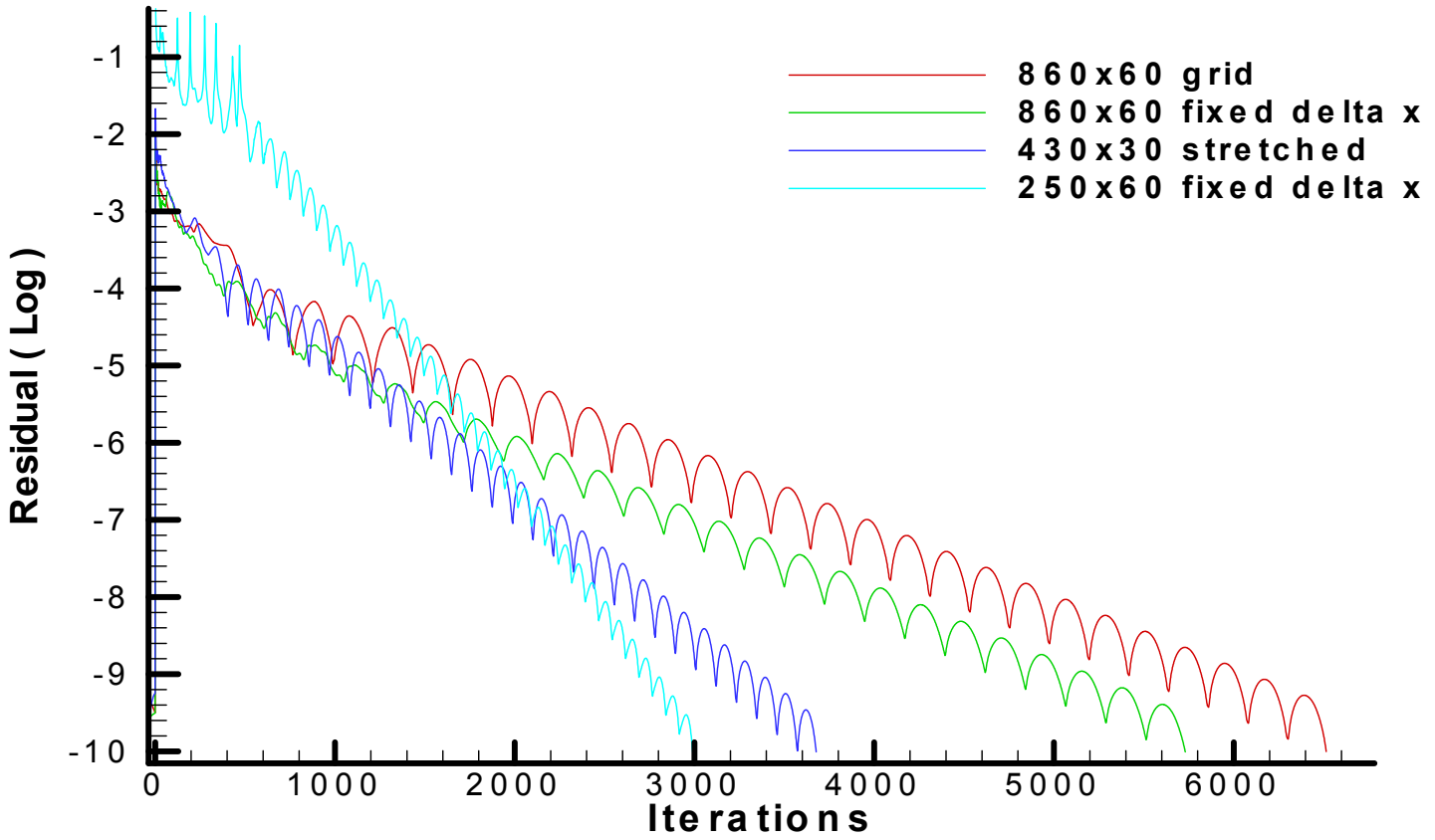

Figure 34: Hydrogen Annulus Convergence Comparison

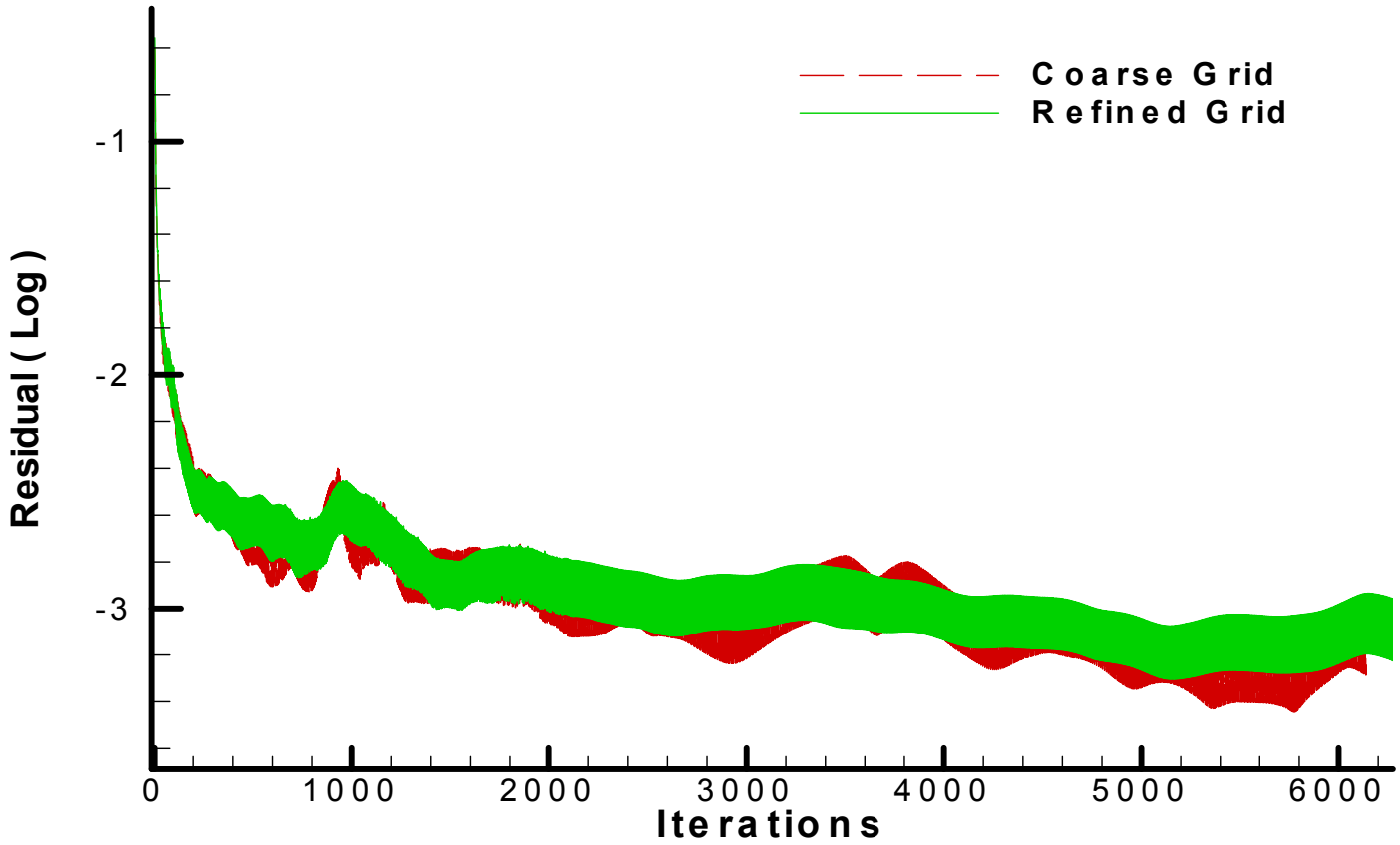

Figure 35: Full Grid Convergence Comparison

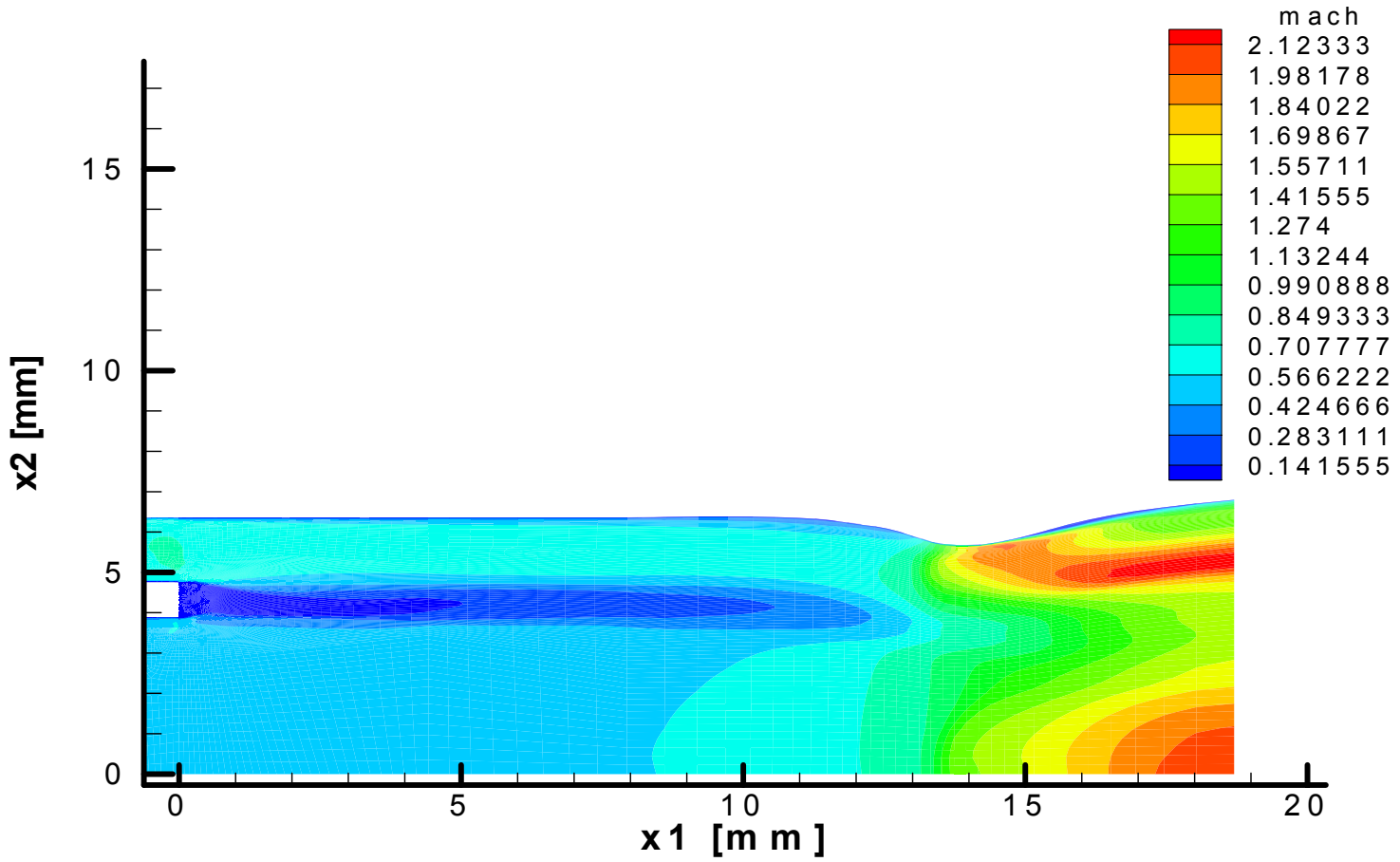

Figure 36: Mach Contour on Refined Grid

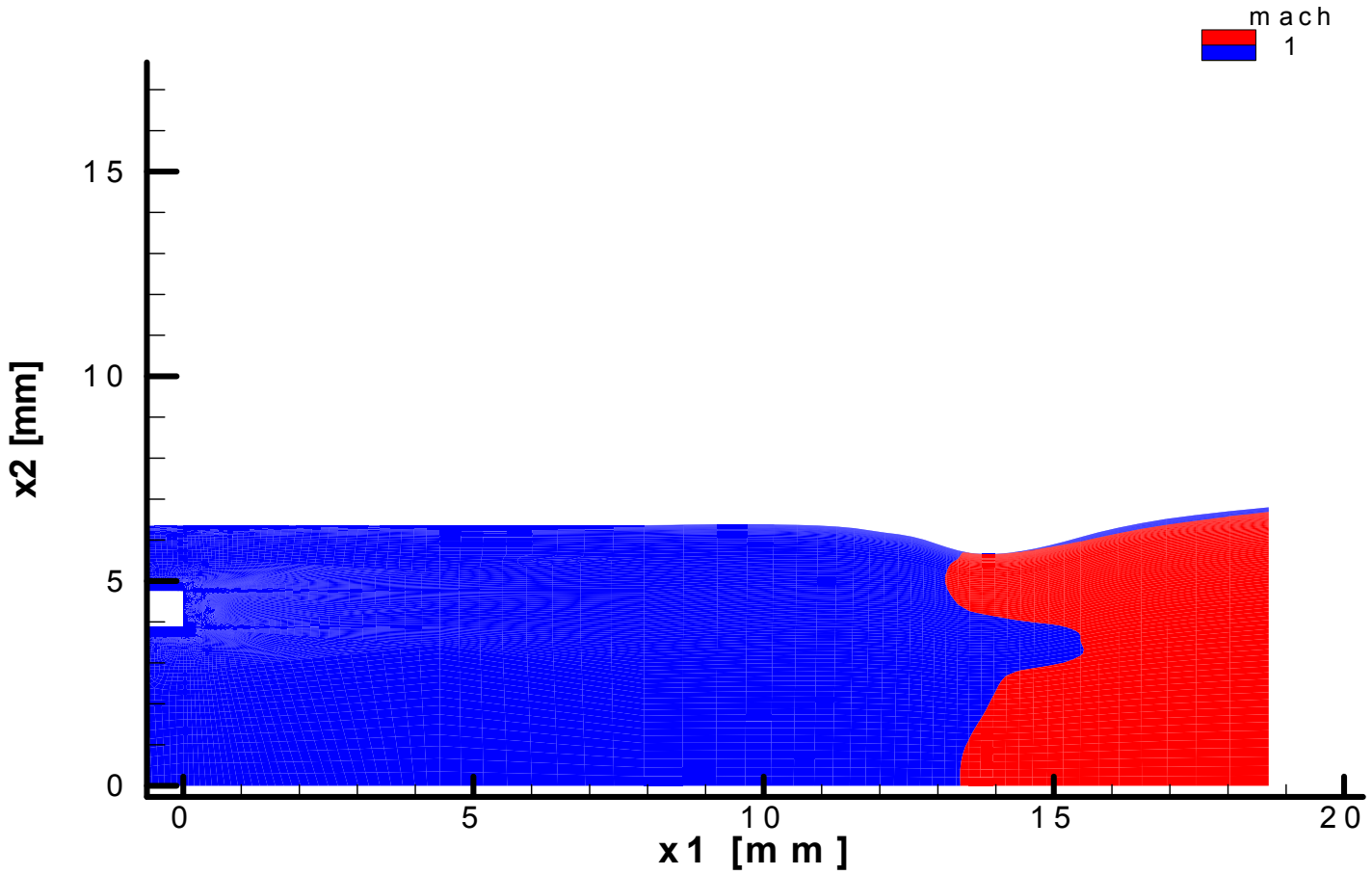

Figure 37: Sonic Line on Refined Grid

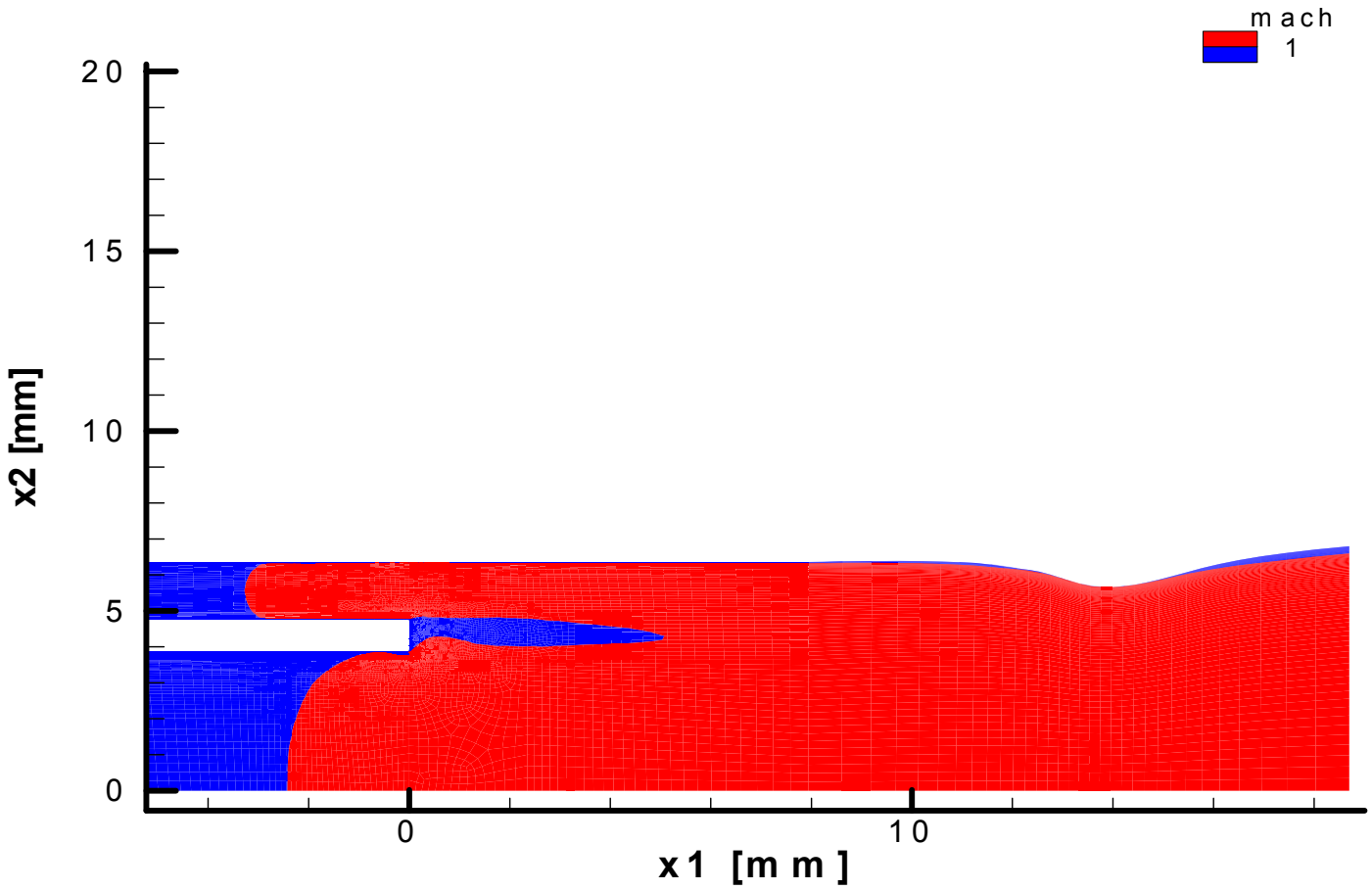

Figure 38: Sonic Line for Cold Flow Case

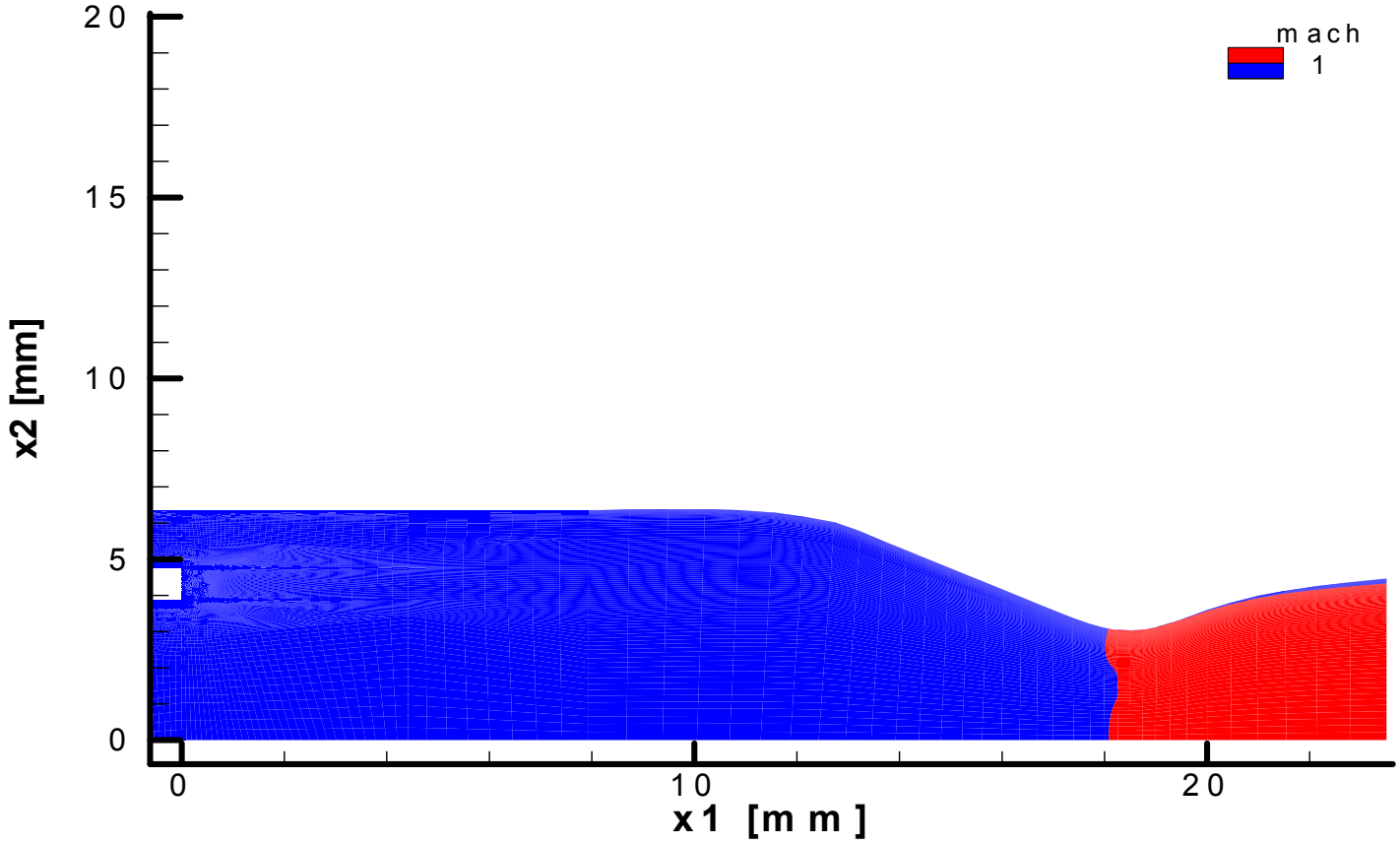

Figure 39: Sonic Line for Cold Flow Case with Choked Throat

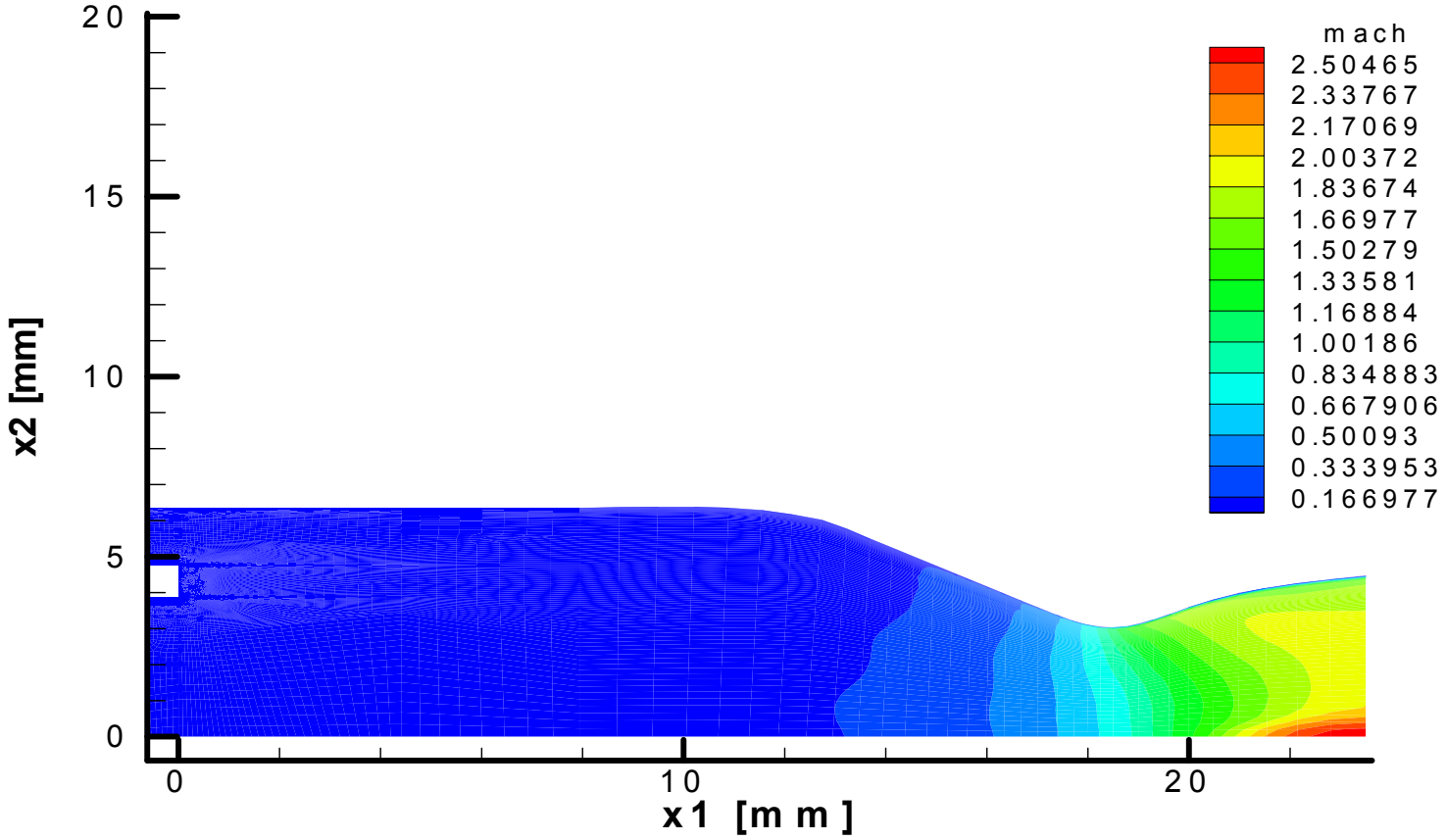

Figure 40: Mach Contour for Reacting Flow on Smaller Throat

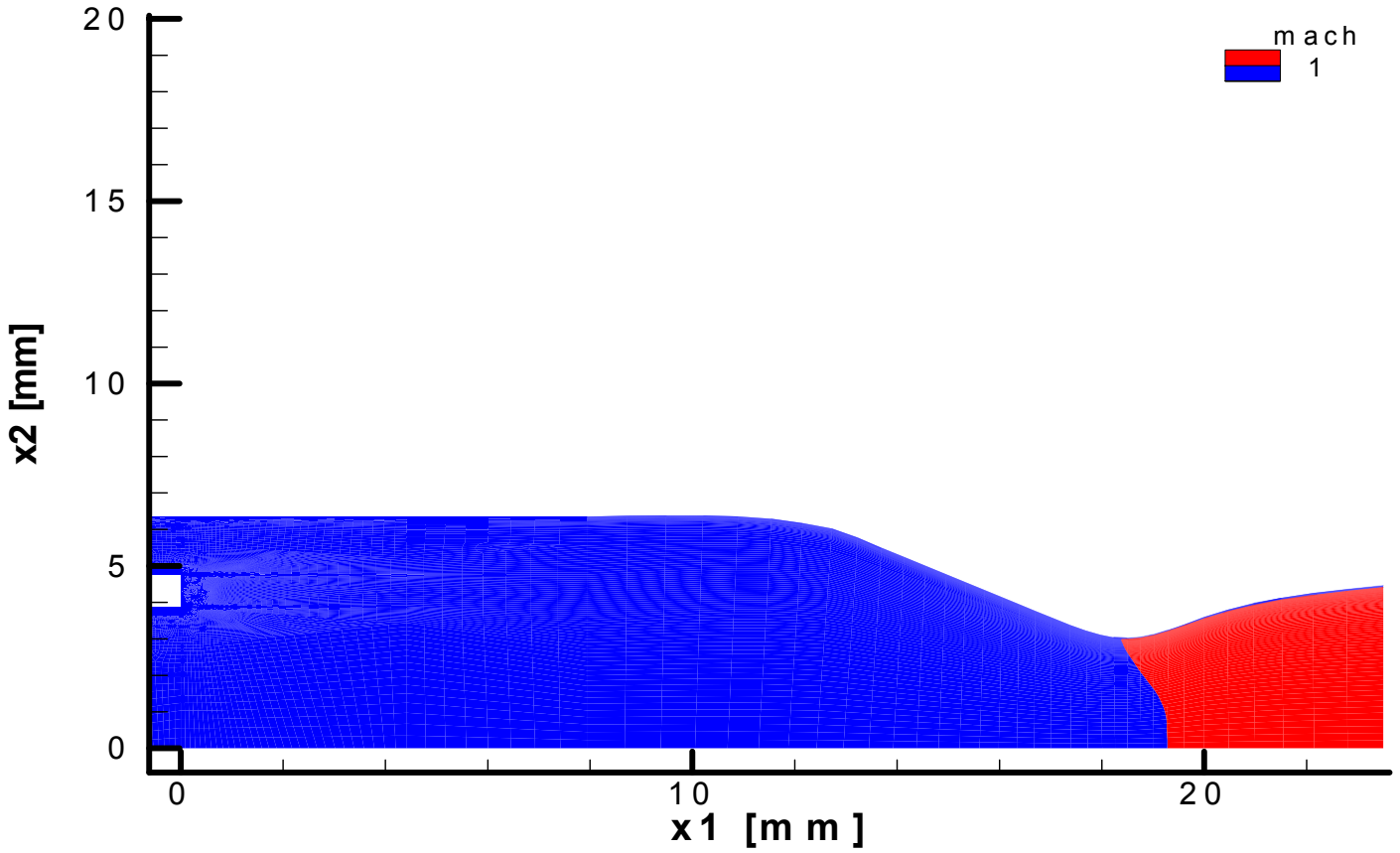

Figure 41: Sonic Line for Reacting Flow on Smaller Throat

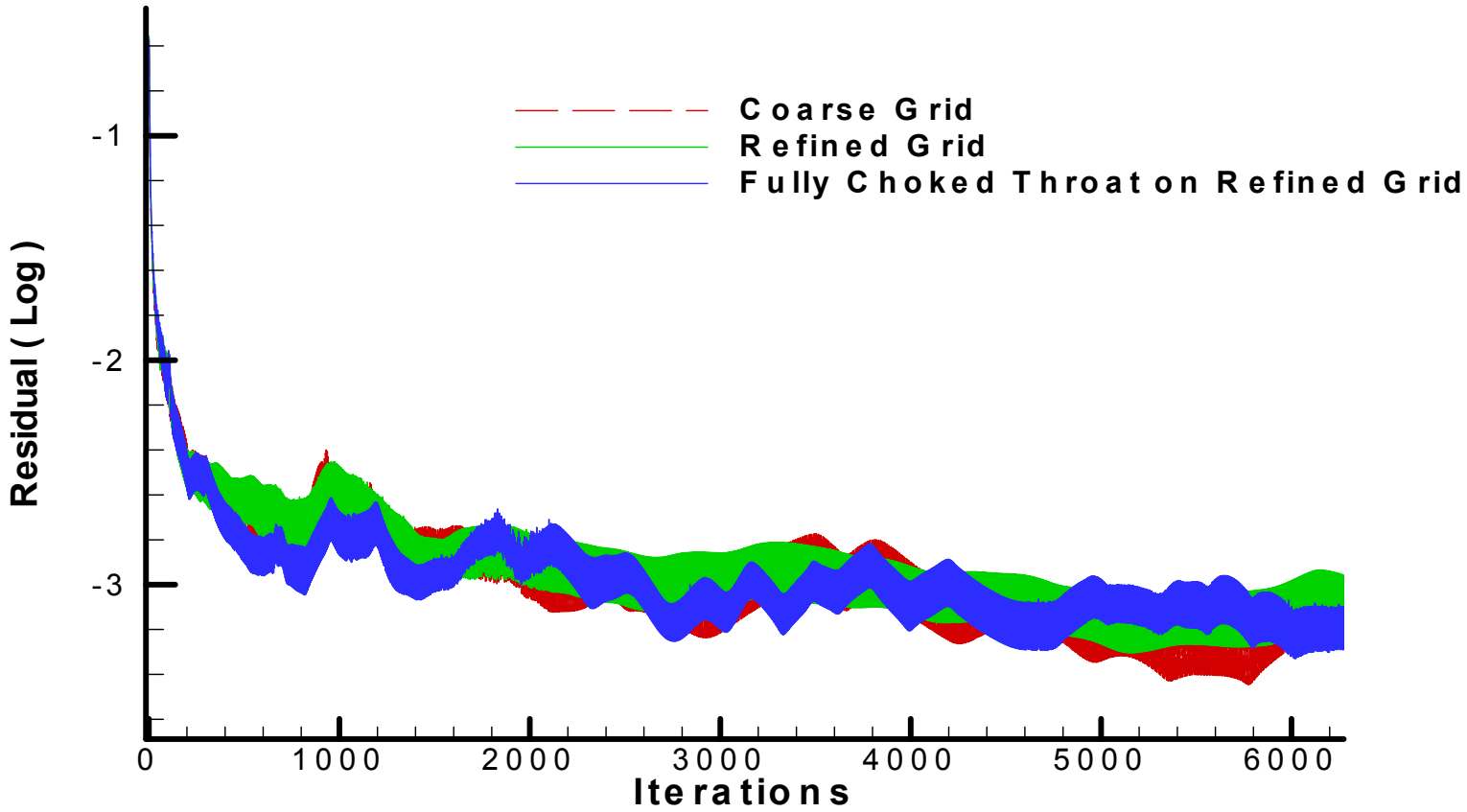

Figure 42: Full Grid Comparison Convergence with Smaller Throat

VITA

Clayton White enrolled in Tennessee Tech University in 1996 as a computer science major only to find that he enjoyed using the computer as a tool to solve math and physics problems. He changed his major to applied physics with a secondary concentration in computer science and did summer research utilizing data acquisition and reduction analysis software in the Gamma Ray Laboratory at the university. After considering several related fields in graduate studies, he chose to attend University of Tennessee Space Institute to study computational fluid dynamics where he could use the computer to solve some of the most difficult of science and engineering problems. He completed his work on the Master of Science in Engineering Science degree in August 2003. Afterwards he plans to study for his doctorate in computational engineering at the SimCenter at the University of Tennessee at Chattanooga.